Contents lists available at ScienceDirect

Arabian Journal of Chemistry

journal homepage: www.ksu.edu.sa

Review article

Recent advances on small molecule doped carbon nitride photocatalysts: Application in environmental water remediation and clean energy production

Tianyu Zhou [a,c,e], Guangbo Che [a,d], Chunbo Liu [a,c,*], Lan Ding [b,*], Honghui Teng [a,c,*]

[a] Key Laboratory of Preparation and Application of Environmental Friendly Materials, Ministry of Education, Jilin Normal University, Changchun 130103, PR China
[b] State Key Laboratory of Inorganic Synthesis and Preparative Chemistry, College of Chemistry, Jilin University, Changchun 130012, PR China
[c] Jilin Joint Technology Innovation Laboratory of Developing and Utilizing Materials of Reducing Pollution and Carbon Emissions, Jilin Normal University, Siping 136000, PR China
[d] Baicheng Normal University, Baicheng 137000, PR China
[e] Jilin Province Product Quality Supervision and Inspection Institute, Changchun 130103, PR China

ARTICLE INFO

Keywords:
Photocatalysis
Carbon nitride
Small molecule doping
Environmental water remediation
Clean energy production

ABSTRACT

Sustainable photocatalytic clean energy production and environmental water remediation technologies represent effective strategies for mitigating energy and environmental crises. The key to successful implementation of photocatalysis lies in the choice of a suitable photocatalyst. Carbon nitride (CN or g-C_3N_4), as a metal-free semiconductor, has been extensively utilized in photocatalytic energy conversion and environmental purification due to its stable physicochemical properties, cost-effective materials, straightforward preparation method and tuneability of structure/band-gap. However, CN faces challenges such as limited visible-light absorption, insufficient exposure of active sites, and high recombination rate of photogenerated carriers. Doping has emerged as an efficient strategy to enhance the photocatalytic activity of CN, particularly through small molecule doping, and numerous research reports have been reported in recent years, while there is no specialized reviews to summarize them. This paper provides a comprehensive summary of the research progress on small molecule doping for improving the catalytic activity of CN including the formation of CN skeleton (e.g., benzene ring, heterocyclic ring, small molecule bonding), via doping elements from small molecules (B, S, O, C, Cl, P) as well as defect formation induced by small molecule doping. At last, the current challenges and future prospects in this field are discussed.

1. Introduction

In recent decades, the rapid advancement of industrialization and urbanization has led to extensive consumption of fossil fuel involving coal, petroleum and natural gas, which has resulted in a global energy shortage, climate warming, frequent extreme weather events, significant damage to the ecological environment, and poses serious threats to human health (Jatoi et al., 2023, Li et al., 2022b, Nagella et al., 2023, Palani et al., 2022, Yan et al., 2023). Furthermore, the exponential growth in population along with accelerated industrialization/urbanization have contributed to an increased demand for industrial chemicals, pharmaceuticals, and personal care products aimed at enhancing quality of life (Chen et al., 2023, Kuspanov et al., 2023, Zheng et al., 2023). However, improper usage and indiscriminate discharge of these substances exacerbate the continuous spread of resistance genes leading to environmental pollution while also posing risks to human health and other organisms (Yang et al., 2020). The ongoing environmental crisis and energy scarcity have long hindered sustainable development in contemporary society while contradicting efforts towards achieving carbon peak and carbon neutrality (Chen et al., 2022, Lin et al., 2022). Therefore, there is an imminent imperative for the advancement of sustainable clean energy production technologies alongside environmental water remediation methodologies (Ramin Babazadeh and Nastaran 2023a, b, Wang et al., 2022b), for example, the pursuit of zero-emission and high-energy renewable hydrogen as a substitute for heavily polluting fossil fuels, and the development of fuel cells, supercapacitors, photocatalysts, solar cells, among others (Li et al., 2022a, Ma et al., 2024, Zhang et al., 2022b).

* Corresponding authors.
E-mail addresses: chunboliu@jlnu.edu.cn (C. Liu), dinglan@jlu.edu.cn (L. Ding), tenghonghui@jlnu.edu.cn (H. Teng).

https://doi.org/10.1016/j.arabjc.2024.105808
Received 14 March 2024; Accepted 23 April 2024
Available online 25 April 2024

Photocatalytic solar energy conversion technology possesses the merits of high efficiency, environmental friendliness, and cost-effectiveness, making it recognized as one of the most effective strategies for mitigating environmental crisis and energy scarcity (Ismael 2021, 2022b, Jiang et al., 2021b, Ma et al., 2022). As commonly acknowledged, the photocatalytic process typically encompasses three sequential steps (Fig. 1**a**), namely light absorption and utilization, efficient separation and migration of photogenerated charge carriers (e^-/h^+, ready to occur via bulk recombination and migration to surface recombination), and subsequent redox reactions occurring at the surface of photocatalysts. Under sunlight illumination, semiconductor photocatalysts drive photocatalytic reactions to generate active species such as photogenerated carriers (h^+ and e^-) and free radicals ($\bullet O_2^-$, $\bullet OH$, $^1O_2$, etc.). These active species migrate the surface of semiconductor to photodegrade pollutants and photocatalytic water splitting to generate hydrogen, realizing environmental remediation and clean energy production (Fig. 1**b**) (Che et al., 2023b, Noureen et al., 2023, Zhou et al., 2022b). Therefore, the successful implementation of this technology relies heavily on the preparation of efficient, durable, cost-effective, environmentally friendly, and stable photocatalysts.

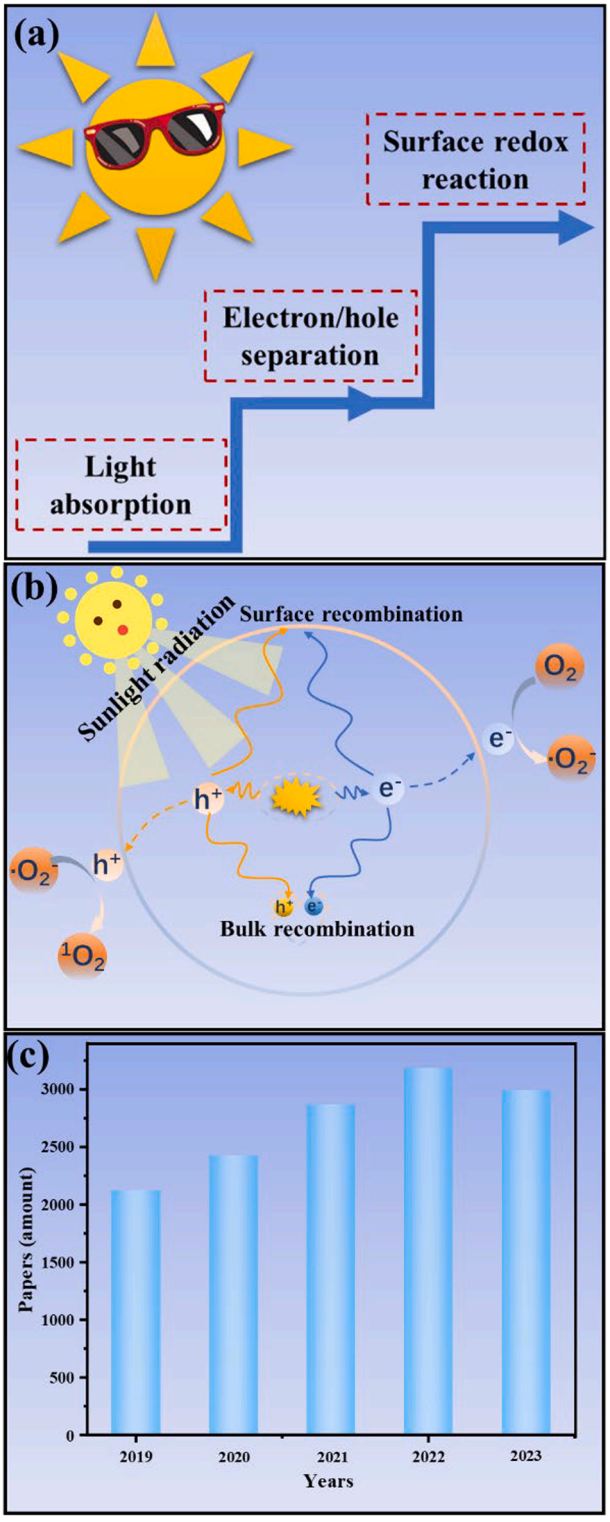

Fig. 1. Scheme of the sequential steps of photocatalytic reaction (a). Scheme of photoexcitation and charge transfer pathways (b). The number of publications per year in the past five years concerning the topic "photocatal* and carbon nitride" (c).

Photocatalysts are primarily categorized into inorganic and organic semiconductor photocatalyst. Among them, inorganic semiconductor photocatalysts mainly comprise metal oxides (e. g., Fe_2O_3, ZnO, Cu_2O) (Chen et al., 2021b, Peng et al., 2024, Zhang et al., 2024), metal sulfide (e.g., CdS, MoS_2) (Lu et al., 2022), Ag-based photocatalyst (e.g., Ag_2S, Ag_3PO_4) (Zhang et al., 2023a) and Bi-based photocatalyst (e.g., BiOX, X = Cl, Br, I) (Guan et al., 2021). Many of the aforementioned inorganic photocatalytic materials have been studying in depth, while hindered by some challenges such as heavy metal leakage, photocorrosion, and high cost (Lu et al., 2019, Peng et al., 2019). In contrast, organic semiconductor photocatalytic materials reveal virtues including high π electron delocalization, potentiality with low cost, absence of metals while being easily modifiable. Carbon Nitride (CN or g-C_3N_4) among them stands out for material scientists as well as environmental and energy scientists due to its adjustable structure/band-gap properties along with simple synthesis methods using readily available raw materials at a low cost while maintaining stable physicochemical characteristics (Ismael 2023a, Liu et al., 2022a, Rana et al., 2022, Zhou et al., 2022b). Specifically, CN, as a type of non-metallic semiconductor polymer material, whose structure only contains two highly abundant elements: C and N (Ismael and Wark, 2022, Praus, 2022). The main raw materials used for its preparation are inexpensive nitrogen-rich substances like urea, melamine or dicyandiamide, making it quite economical to produce (Wang et al., 2022c). Additionally, the bandgap width of CN is appropriate and adjustable straddling both sides of H^+/H_2 reduction potential as well as H_2O/O_2 reduction potential, meeting the thermodynamic requirements for the generation of common oxidizing species and photocatalytic hydrogen/H_2O_2 production (Ismael 2020a, 2022a). The bandgap measures approximately 2.7 eV exhibiting obvious visible light response (Ismael and Wu, 2019, Ismael et al., 2019, Liu et al., 2020). These merits make CN holding immense application prospects within the field of photocatalysis, such as photodegradation (Jin et al., 2022, Zeng et al., 2023), coupled persulfate oxidation degradation (Ni et al., 2022), self-Fenton (Jing et al., 2023), hydrogen energy production (Li et al., 2021b, Zhou et al., 2022a), hydrogen peroxide production (Che et al., 2021a), nitrogen fixation (Dong et al., 2022a), biomass conversion (Wu et al., 2021b, Yang et al., 2022), antibacterial (Zeng et al., 2020b) and other applications. However, the single CN also suffers from several limitations (Ismael 2020b). Firstly, the layered stacking structure of CN limits its specific surface area and hinders photocatalysis performance by restricting exposure to active sites in photocatalytic reactions (Dong et al., 2021a, Ruan et al., 2022). Secondly, high exciton binding energy leads to severe recombination of photogenerated electrons and holes, while sluggish migration kinetics of photogenerated charges results in the annihilation of active species before they migrate to the catalyst surface. Lastly, visible light utilization is insufficient in terms of both range and intensity (Wu et al., 2022, Zhang et al., 2015).

Focus on the aforementioned issues, researchers have adopted diverse strategies for modifying CN, including morphology regulation (Wu et al., 2022), doping (Jiang et al., 2021b, Wang et al., 2021a), heterostructure construction (Zhou et al., 2023b), loading precious

metals (Zhong et al., 2022), crystallinity regulation (You et al., 2023), among others (Bai et al., 2022, Ismael 2023b, Khayoon et al., 2023, Patnaik et al., 2021, Sun et al., 2021). The substantial increase in CN-related research publications on the Web of Science (WOS) corroborates this observation, with over 2000 publications per year in the past five years (Fig. 1**c**). Notably, doping with small molecules has been found to effectively enhance the catalytic activity of CN (Hu et al., 2020, Lei et al., 2021, Zhang et al., 2021, Zhang et al. 2020c, Zhou et al., 2022b). Due to the diverse range of small molecules available, the CN framework can be tailored by carefully choosing small molecules with specific structures for precise control skeleton arrangement, elemental doping, and defect engineering, so as to finely tune the CN electronic structure, light absorption properties, charge behavior, ultimately enhancing catalytic activity of CN. In recent years, there have been an ocean of reports on enhancing the catalytic activity of CN through small molecule doping, and our group has conducted several series studies that have demonstrated the effectiveness of this method (Chen et al., 2023, Jiang et al., 2023, Wang et al., 2023, Yan et al., 2021, Zhou et al., 2023a, Zhou et al., 2023b, Zhou et al., 2022b). Although several excellent reviews have included doping-type CN (Ma et al., 2024, Nagella et al., 2023, Patnaik et al., 2021, Wang and Shen 2020) (Kumar et al., 2021, Patnaik et al., 2021, Xing et al., 2021), while there is currently no specialized review available summarizing small molecule doped CN. To maximize the photocatalytic activity of CN and provide a valuable reference for researchers, it is crucial for the scientific community to stay updated with the latest developments and trends in small molecule-doped CN photocatalysts and their contributions in environmental water remediation and clean energy production.

Based on the above discussion, this article aims to provide a comprehensive summary of recent advancements (mainly from 2019 to date) in enhancing the photocatalytic activity of CN through small molecule doping, specifically focusing on its application in clean energy production and environmental water remediation. The review mainly includes (Fig. 2) the incorporation of small molecules to form the CN skeleton (including benzene ring, heterocycle, and small molecule bonding, etc.), elements doping via small molecules (B, S, O, C, P, etc.) and defect formation via doping small molecules (Fig. 3). Furthermore, the current challenges and future prospects in this direction were discussed. It is important to note that while several reviews on CN modification have been published (Kumar et al., 2021, Patnaik et al., 2021, Xing et al., 2021), this particular review distinguishes itself by exclusively discussing element doping and defects induced by small molecule doping. This comprehensive overview serves as a valuable resource for researchers seeking to stay abreast of the latest developments and trends pertaining to applications of small molecule-doped CN photocatalysts in environmental water remediation and clean energy production.

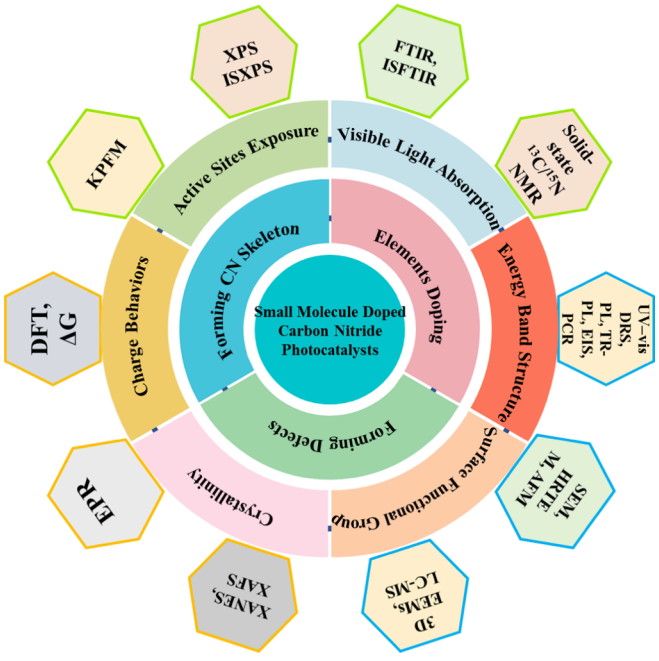

Fig. 2. Small molecule doping to improve CN photocatalytic performance discussed in this review.

2. Strategies for small molecule doping

2.1. Form CN skeleton

2.1.1. Benzene ring doping

The common structure of CN is composed of 3,s-triazine units, which are connected to form a typical 2D structure. The benzene ring is all-carbon aromatic properties and larger delocalized π bonds, revealing higher delocalized electronic properties (Zhou et al., 2019a). Incorporating the benzene ring into the conjugated polymer network of CN not only expands its conjugation effect but also regulates its internal electronic structure (Chen et al., 2020a, Lin et al., 2021a, Sun et al., 2019c, Yu et al., 2017, Yuan et al., 2021, Zhang et al., 2020a), thereby facilitating charge migration and separation within CN while inhibiting photogenerated carrier recombination (Che et al., 2021b, Jiang et al., 2021a, Li and Zhang, 2018, Sun et al., 2019b). Since Professor Wang first demonstrated that co-polymerization of barbituric acid and urea significantly enhances photo utilization and catalytic performance of CN (Qin et al., 2015), numerous studies have been conducted to incorporate benzene rings (such as benzoic acid, phenylurea, trihydroxybenzene, etc.) into CN frameworks to adjust CN light absorption and electronic structure, and promote their catalytic activity (Zhang and Wang, 2013, Zhou et al., 2019a).

The group led by Professor Zhang fabricated a series CNs with boosted charge transfer and separation efficiency for hydrogen evolution reaction (HER) via doping acetylacetone or aromatic rings into CN (Wang et al., 2018, Xu et al., 2020). Using trimesic-acid and melamine as raw materials, Yuan et al. prepared trimesic-acid doped CN material with benzene ring nesting by hydrothermal precursor method. The insertion of the benzene ring in the CN structure broadened the π-conjugated system of CN, reduced band gap, and broadened the visible-light response range. Meanwhile, the benzene ring served as a receptor to catch photogenerated electrons, promoting effective separation of photo generated charges. The HER rate of the optimal sample was 21.8 times that of pure CN (Yuan et al., 2021). Similarly, Jia et al. prepared capel CN using dicyandiamide and p-phenylenediamine as raw materials through copolymerization. The insertion of the benzene ring replaced the heptazine structure of CN, resulting in an asymmetric local structure. The electronic structure was readjusted to form independent positive–-negative charge centers and a local internal field, which was significantly conducive to the separation of photogenerated excitons. The HER rate of this material was ten times that of original CN with the apparent quantum yields (AQE) at 400 nm and 420 nm reaching 11.3 % and 9 %. This study indicates that the insertion of the benzene ring generated a photoelectric synergistic effect, changed the local charge distribution and electron transfer kinetics, and promoted the improvement of HER (Jia et al., 2019).

Through a simple thermally induced copolymerization method, our research group synthesized a CN photocatalyst with efficient charge separation and porous morphology employing m-aminophenol and urea as raw materials. The doping of m-aminophenol introduced a benzene ring into the CN structure, which not only regulated the morphology of the CN (porous layered structure), but also formed an integrated intramolecular donor–acceptor (D-A) structure. This structure greatly enhanced the driving force of photogenerated exciton separation, improved the dynamics of photogenerated charge transport, and

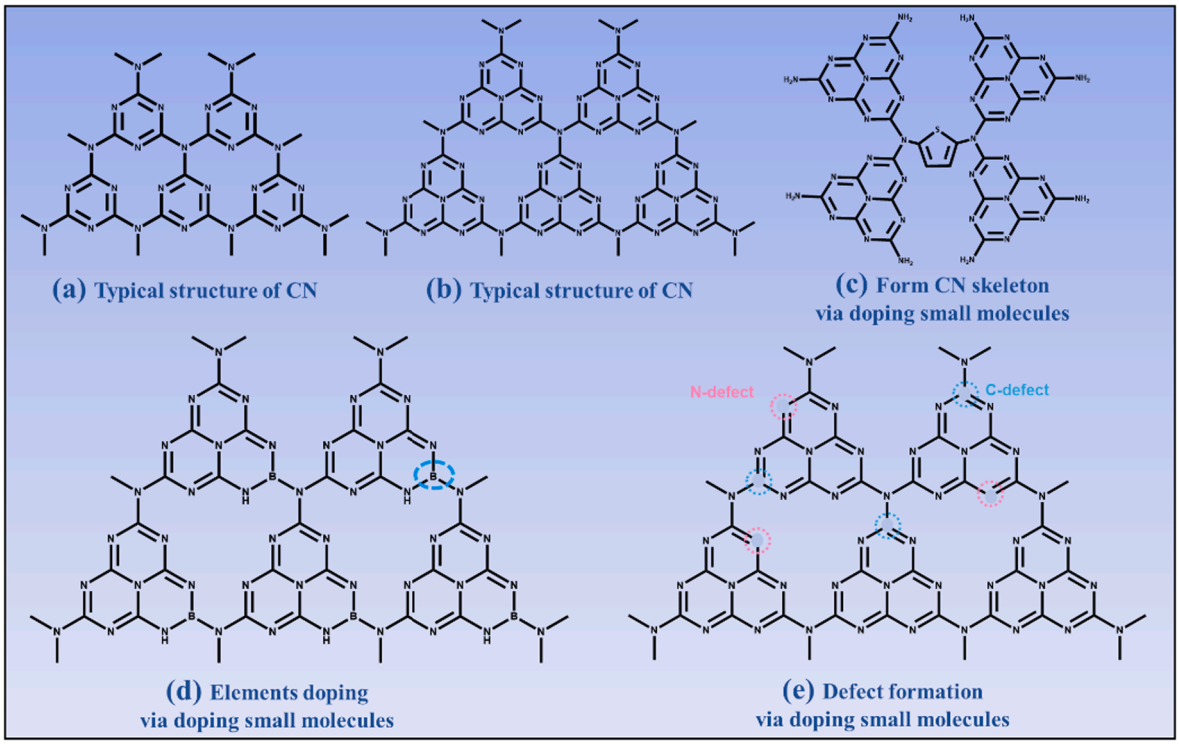

Fig. 3. Typical structure of CN (a and b). Typical structure of small molecules doped CN, form skeleton (c, example of thiophene doping), elements doping (d, example of B doping) and defect formation (e, N and C defect).

reduced the recombination of carrier. In addition, the introduction of benzene ring also expanded the delocalization range of π electrons and promoted visible light absorption (Jiang et al., 2021a, Zhang et al., 2020b, Zhou et al., 2019a). The optimal HER rate and photodegradation rate of CN doped with m-aminophenol were increased by 2.73 and 5.3 times compared to pure CN (Zhou et al., 2022b). In addition, Kim et al. [67] proposed a simple method of incorporating benzene rings into CN by using benzoic acid as a dopant and replacing the nitrogen of the tertiary amine in CN with a benzene molecule connected by three heptriazine rings (Kim et al., 2017). The doping of benzene ring transformed the planar symmetric molecular structure of CN into a twisted geometric structure, propelling the separation of photogenerated charge and delaying the recombination of photogenerated carrier. The doping of the benzene ring also formed a new skeleton for CN, reducing the π-π* transition of the conjugated ring system. However, due to planar geometric distortion, more nitrogen atoms and lone pair electrons were exposed, promoting the n-π* transition. Compared with the original CN, benzene doped CN materials have higher photocurrent and lower charge transfer impedance, indicating more effective separation of photogenerated charges.

2.1.2. *Aromatic heterocyclic doping*

Doping organic monomers with different aromatic heterocycles into CN frameworks to improve the photocatalytic performance of CN has been extensively favored by researchers (Ge et al., 2021, Zhou et al., 2019a). On the one hand, aromatic rings can broaden the range of CN conjugated systems and facilitate electron delocalization (Guo et al., 2018, Li et al., 2018, Sun et al., 2019b). On the other hand, heteroatoms can effectively improve charge behavior, generate more charge transition modes, and improve light absorption (Ge et al., 2021, Zhou et al., 2019a).

2.1.2.1. Nitrogen heterocyclic doping. Numerous studies have proven that small molecules doped with conjugated nitrogen heterocycles can not only increases the π electron density of CN and allows more electrons to participate in the proton reduction process (Chen et al., 2019, Liang et al., 2021, Qin et al., 2015), but also utilizes the negative induction effect of N atoms in the heterocycle to graft the heterocycle structure onto the edge of the CN structure, thus promoting the directional migration of photogenerated charges and avoiding the recombination of photogenerated carriers (Dong et al., 2021b, Li et al., 2021a). Li et al. used hydrothermal method to assemble monomers melamine and niacin with carboxyl and pyridine rings into strip-shaped supramolecules through hydrogen bonding, and calcined them to obtain one-dimensional banded CN (Liang et al., 2021). The obtained material exposed more active sites, and possessed delocalized large π bonds, which increased the π electron density, narrowed the band gap and accelerated charge/mass transfer. The HER rate under visible light irradiation (126.2 mol h^{-1}) was much higher than that of CN (7.2 mol h^{-1}), and the AQE at 420 nm reached 6.81 %.

Furthermore, lone pair electrons on N atoms can activate n-π* electron transitions of CN, broadening visible light absorption over 500 nm and generating intermediate states (Jiang et al., 2023, Wan et al., 2022). Our team also explored the performance of nitrogen heterocyclic modified CN (Fig. 4**a-e**). For example, a pyrazine doped twisted structure CN with awakened n-π* electron transitions was customized by thermally induced copolymerization of pyrazine 2,3-dicarboxylic acid and urea via one-pot thermal-melt assembly (Jiang et al., 2023). A series of characterization tests showed that the optimized catalyst has improved visible-light utilization (Fig. 4**a and 4b,** $\lambda > 500$ nm), sufficient exposure of active sites (higher specific surface area), and hybrid electronic structure (significantly enhanced charge behavior). Similarly, Professor Cao constructed D-A integrated CN copolymer via one-pot thermal polycondensation of urea and small π-conjugated molecule 5,8-DibroMoquinoxaline (Fig. 5**a**) (Wan et al., 2022). A series of characterizations (e.g., XRD, FTIR, Fig. 5**b-e**) and DFT calculations confirm the electron D-A modulation created an internal electric field to promote the intramolecular charge transfer (ICT, Fig. 5**j**) from 5,8-DibroMoquinoxaline segment (electron donor) to the tri-s-triazine ring (electron acceptor). Due to the spatial isolation of LUMO/HOMO, expanded p-π

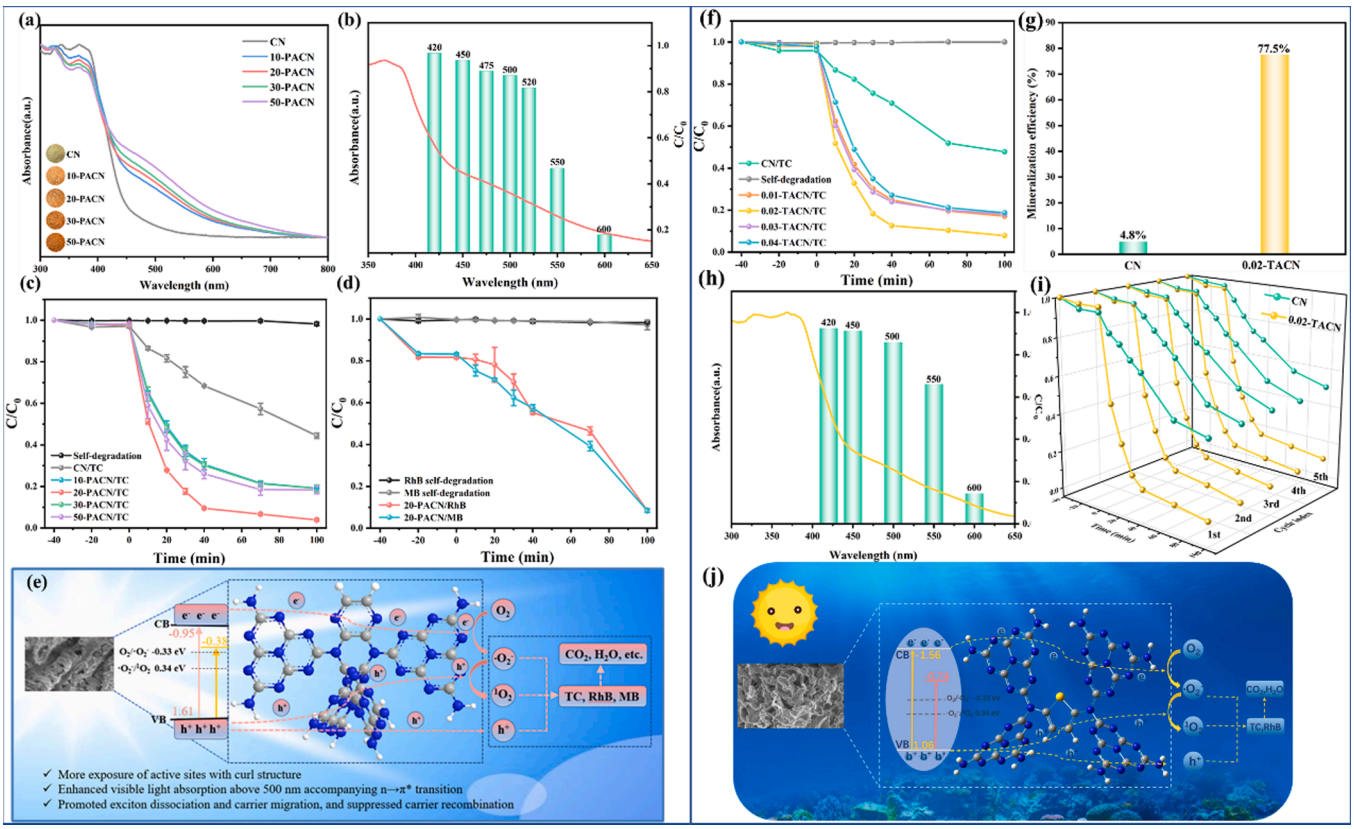

Fig. 4. UV–Vis DRS spectra of all products (a). Wavelength-dependent TC photodegradation rate via 20-PACN (b). Photodegradation performance of all products for TC (c). Photodegradation performance of 20-PACN towards MB and RhB (d). Schematic illustration of the propelled photodegradation mechanism over 20-PACN (e). Copyright 2023 Elsevier (Jiang et al., 2023). Photodegradation performance of all products (f). The TOC removal efficiency of TC (g). Wavelength-dependent TC photodegradation rate via 0.02-TACN (h). Cycling photodegradation performances (i). Schematic illustration of the propelled photodegradation mechanism over 0.02-TACN (j). Copyright 2023 Elsevier (Shi et al., 2023).

conjugate, lower $\triangle G_{H+}$ (Fig. 5**f**) and appropriate midgap states with inherent band gap, the best HER rate reached 3012.5 μmol $g^{-1}h^{-1}$ under $400 < \lambda < 800$ nm visible light irradiation (about 3.3 times that of single CN, Fig. 5**g**) and comparable stability (Fig. 5**h-i**).

Edge nitrogen heterocycles can broaden the edge conjugation effect of CN and promote the delocalization effect of charge separation. It also induces electrons to migrate outward to the edge of CN, effectively preventing the recombination of photogenerated carriers and dramatically improving the photocatalytic activity of doped samples (Dong et al., 2021b, Li et al., 2021a, Teng et al., 2019). Typically, utilizing a one-pot thermal-polymerization method, Professor Li grafted the pyridine ring in 2-aminopyridine onto the edge of the CN framework as a conjugated nitrogen heterocycle (Fig. 6**a-f**)(Li et al., 2021a). The pyridine ring, as an electron withdrawing group, can transfer electrons from the center to the edge of the CN framework, promoting dissociation of excitons. The doping of pyridine ring played a dual regulatory role in the electronic structure hybridization and electron directed transfer of CN, effectively suppressing the recombination of photogenerated carriers and greatly enhancing the HER performance (Fig. 6**f**). The HER rate of the best sample was as high as 6317.5μ mol $g^{-1}h^{-1}$, which is 3.9 times that of pure CN (Fig. 6**a**). The AQE at 420 nm was as high as 20.1 % (Fig. 6**b**). In addition, the group also developed a g-C_3N_4-4AAP photocatalyst by polymerizing urea with 4-aminoantipyrine (4-AAP) (Dong et al., 2021b). Diazole has a heterocyclic structure of methyl hypercoupling and benzene ring coupling. Grafting the unique conjugated diazole bond onto the edge of the CN framework can generate strong edge induction and delocalization effects, which can improve the dissociation of charge carriers and prolong their lifetime, thereby driving HER reactions. The HER rate of the best product was 284.2 2 μmol h^{-1}, which was 10 times higher than pure CN, and the AQE at 420 nm was as high as 24.2 %. Similarly, via doping pyrimethamine into CN with a facile one-step polymerization method, the group constructed a cross-linked bridge CN frame through a multi-bonding mode broadening the visible light utilization, and accelerating the migration and dissociation of photogenerated excitons via extending π-conjugated channel (Zhang et al., 2022c).

2.1.2.2. Sulfur heterocyclic doping. Similar to doped nitrogen heterocycles, doped sulfur heterocycles into CN can also broaden the range of π electron conjugation. More obviously, there are two lone electron pairs on the sulfur atom, which can promote n-π* transition of CN, enhancing visible light absorption and photocatalytic activity (Ge et al., 2021, Guo et al., 2019). In addition, as a typical electron rich ligand, thiophene in the sulfur heterocycle is easily grafted onto the CN skeleton, constructing an integrated intramolecular D-A structure to enhance exciton dissociation and carrier migration dynamics (Liu et al., 2022c).

Professor Ao prepared a porous CN based donor-π-acceptor organic conjugated polymer by copolymerizing 5-bromothiophene-2-formaldehyde with urea. This polymer extended the π-conjugated range, introduced a rich porous structure, and remarkably propelled intramolecular charge migration, light utilization and mass transfer of pollutants, prominently improving the photodegradation performance (Che et al., 2023a). Professor Zhang has prepared a novel CN photocatalyst grafted with 5-bromo-2-thiophene formaldehyde with a D-A structure. Compared with CN, the apparent rate constant of photodegradation of oxytetracycline by this material was increased by 2.43 times, and the degradation efficiency was as high as 93 %. After 60 min of photodegradation reaction, the removal efficiency of TOC reached 38 %, which is attributed to the acceleration of intramolecular charge

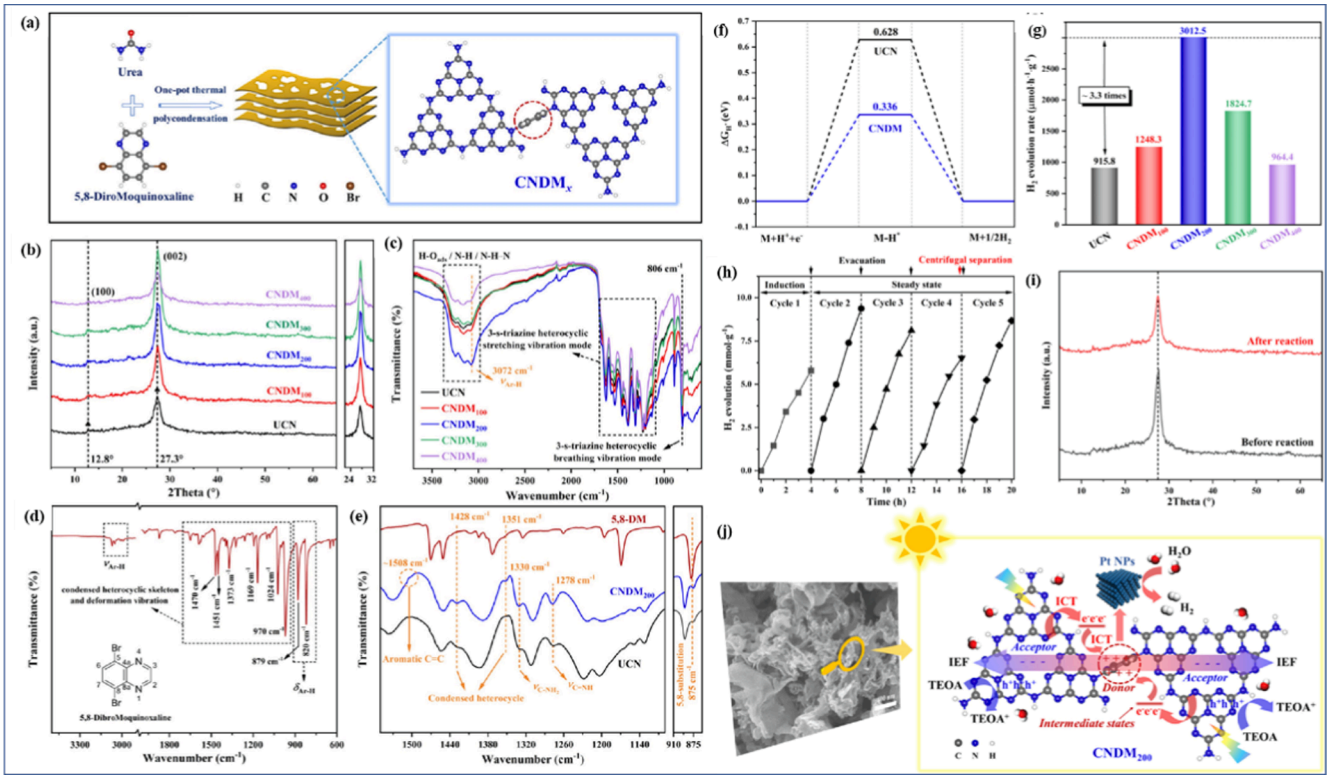

Fig. 5. Schematic illustration of material synthetic process (a), XRD patterns (b), FTIR spectra (c), FTIR spectra of 5,8-DibroMoquinoxaline molecule (d), magnified FTIR spectra (e). Gibbs free energy for the adsorption of single H atom at samples (f); HER rates of all samples (g); HER stability test (h); XRD patterns before and after stability test (i); Schematic illustration of possible HER mechanism (j). Copyright 2022 Elsevier (Wan et al., 2022).

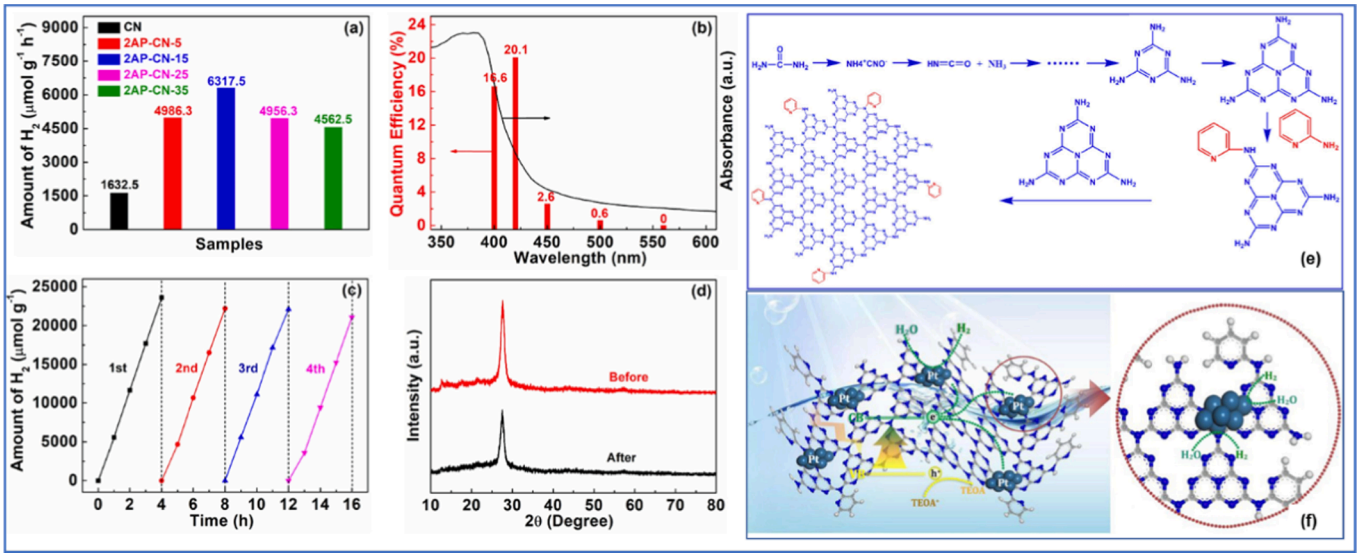

Fig. 6. HER rates of all samples (a); AQE values (b), HER cycles (c), XRD patterns before and after HER cycles (d). The possible polymerization reaction schematic of photocatalyst (e). The possible HER mechanism (f). Copyright 2021 Elsevier (Li et al., 2021a).

separation and controllable electron migration (Zhang et al., 2022a).

Our group prepared ultra-thin CN nanosheets with intramolecular D-A structure and awakened n-π* transition through a one-pot thermally induced copolymerization reaction after completely grinding of urea and 2,5-thiophene dicarboxylic acid (Fig. 4**f-4j**) (Shi et al., 2023). A series of characterization tests confirmed that the best product had an absorption edge of 670 nm (Fig. 4**h**), a specific surface area of 98.3 m^2/g, and significantly enhanced charge transfer compared to CN. The sample can photodegrade 92.1 % of TC, 100 % of RhB (Fig. 4**f**). TOC removal rate reached 77.5 % for TC, which evidently higher than 4.8 % of CN (Fig. 4**g**). Quenching experiments and ESR confirmed that h^+,$\cdot O_2^-$ and $^1O_2$ assisted in photodegradation, which benefited from the rise of conduction bands and the presence of intermediate states.

2.1.3. *Small molecule bonding*

The method of participating in CN skeleton is not limited to introducing conjugated structures such as benzene rings and heterocycles, but also introduces small molecules with special functional groups, such

as carboxyl, hydroxyl, amino, aldehyde and other special functional groups. On the one hand, small molecules can be grafted onto the edge of the 3,s-triazine ring through a phenol/aminoaldehyde condensation reaction with the edge amino group of CN. On the other hand, small molecules can participate in ring grafting reactions while forming their own rings or connecting multiple 3,s-triazine rings. In addition, introducing electron donating or electron withdrawing groups into the structure of CN can regulate the internal electronic structure of CN. At the same time, O in carboxyl and hydroxyl groups, and N in amino groups can bind to CN through hydrogen bonds, making the interface contact more compact, and conducive to electron transfer (Kim et al., 2017, Ma et al., 2021, Ouedraogo et al., 2018, Zeng et al., 2020a, Zhao et al., 2021b, Zhao et al., 2019, Zhou et al., 2019a). The most representative small molecule among them is amino acids, which contain carboxyl and amino, and are diverse and readily available.

Using asymmetric supramolecular precursor pyrolysis method, Wu et al. prepared actiniae-like CN beams using L-arginine (L-Arg) and melamine as raw materials (Fig. 7**a-7k**) (Wu et al., 2021a). L-arginine has multiple special functional groups (amino and carboxyl groups), which are wonderful supramolecular assembly units. Through acylation reactions, L-arginine can induce the hydrolysis of melamine to assemble asymmetric supramolecular precursors (L-ArgM14), which can adjust the band structure and active sites of CN (Fig. 7**a-7b**). In addition, new carbon or oxygen-containing functional groups introduced into the synthetic materials (ACN14), and the carbon nitrogen ratio was adjusted to give them a hollow microtubule morphology with adjustable band gaps and ultra-thin pore walls (Fig. 7**d-7e and 7g-7h**). The number of active sites was increased, and the visible light utilization rate was enhanced, resulting excellent hydrogen production ability and selectively oxidized phenylcarbinol to benzaldehyde simultaneously with conversion of 90.9 % and selectivity of 99.7 %. Through an one-step pyrolysis method, Ma et al. prepared CN homojunctions with tubular and porous structures using urea and L-cysteine as raw materials (Ma et al., 2021). This unique tubular structure with coexisting triazine and pyridine units can promote the dissociation of excitons in-plane, and provide more active sites. In addition, the superior electronic structure and morphology reduced the Gibbs free energy of HER, and the HER rate reached 4548.4μ mol $g^{-1}h^{-1}$ (35 times of single CN).

It is highly desirable for doping small molecules to form CN framework, especially for special frameworks such as benzene rings and aromatic heterocycles, which can significantly expand the electron delocalization range and are widely recognized in expanding CN light absorption. The introduction of heteroatoms and their constructed electron push–pull or D-A structures are highly beneficial for regulating charge behavior. Therefore, a synergistic impact on structural and optical properties can be realized.

2.2. Element doping

Small molecule doping can also be used to modify CN through element doping, especially by directly preparing CN through high-temperature calcination. Small molecules may decompose during calcination, leaving some elements to participate in the composition of the CN skeleton or interlayer/in-plane electron transfer. Element doping caused by the dope of small molecule, mainly non-metallic element B, S, O, C, Cl, P, which is extremely effective in regulating the electronic structure and promoting the delocalization of π-conjugated electrons in CN, thereby improving charge mobility and separability. It is worth noting that this review aims to discuss the catalytic activity of CN modified by small molecule doping. Therefore, element doping in this section only discusses the situations where doping elements are provided through small molecules, namely, non-metallic element doping realized by small molecule doping. Unlike the heterocyclic doping caused by small molecule doping mentioned above, the element doping caused by small molecule doping in this section has not been clearly confirmed to be involved in ring formation.

2.2.1. B doping

B atoms have more valence layer atomic orbitals than valence electrons, resulting in B-compounds often containing electron deficient centers. Therefore, B atoms are employed by researchers for doping and modifying CNs (Zhao et al., 2021a). Hong et al. prepared B-doped CN nanotubes through a simple hydrothermal calcination process (Bao et al., 2021). The morphology and structure of B-doped CN were effectively regulated, the degree of graphitization was improved, and ordered nanotubes were formed with a significant increase in specific surface area. At the same time, the level of charges was increased, the recombination of carriers was reduced, and the transient fluorescence lifetime was extended. The optimal HER rate reached 22.1 mmol $g^{-1}h^{-1}$ (64 times that of pure CN).

Via hydrogen bonds self-assembly and calcination, Professor Dong fabricated coral-like B-doped CN with boosted molecular dipole for

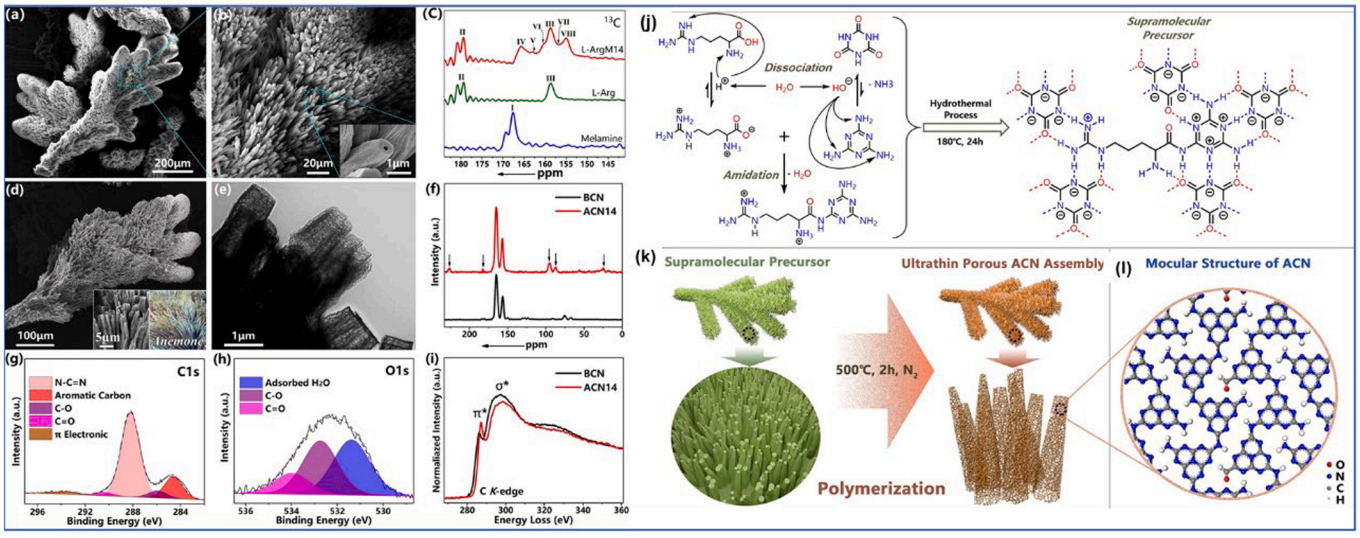

Fig. 7. SEM images of L-ArgM14 (a, b). 13C solid-state NMR of melamine, L-Arg, and L-ArgM14 (c). SEM image of ACN14 (d, the inset is natural anemones). TEM image of ACN14 (e). 13C solid-state NMR spectra of ACN14 and BCN (f). C 1s (g) and O 1s (h) XPS spectra of ACN14. Electron energy-loss spectra near carbon K-edge for BCN and ACN14 (i). Amidation reaction and assembly process between L-Arg, melamine, and cyanuric acid during hydrothermal processes (j). The thermal condensation schematic illustration of supramolecular precursor (k). The molecular structure of ACN (l). Copyright 2021 Wiley (Wu et al., 2021a).

constructing a photocatalysis self-Fenton system (Fig. 8**a-l**) (Jing et al., 2023). The improved molecular dipole of CN stemmed from B heteroatoms doping (Fig. 8**a**). The self-assembly of hydrogen bonding in the raw materials upsets the laminar stacking of CN during calcination, causing the coral-like structure (Fig. 8**b-d**). The coral-like B-doped CN revealed an evidently propelled photocatalytic H_2O_2 generation activity, which was 3.0 times that of pure CN (Fig. 8**i-g**). Furthermore, the photocatalysis self-Fenton activity of coral-like B-doped CN can almost completely degrading 4-chlorophenol with the assistance of Fe^{2+}, and the TOC removal was as high as 70.3 % (Fig. 8**k-l**), which primarily caused by the generation of more strong oxidizing species, i.e., ·OH and h^+, in this collaborative system (Fig. 8**h**).

Through a two-step doping and etching strategy, Du et al. doped B (electronegativity of 2.04 eV) and O (electronegativity of 3.44 eV) into CN with a porous 2D nanostructure. The resulting sample exhibited a typical 2D porous nanostructure with a significantly increased specific surface area and more reactive sites (Du et al., 2021). The B element and O element synergistically control the band gap, accelerating electron transfer, promoting the dissociation of excitons, and prolonging the lifetime of charges/carriers. The HER rate of BO-C_3N_4 nanonet reached 9751μmol h^{-1} g^{-1}, which was nearly 28 times that of single CN, and the AQE reached 8.1 %.

Our team constructed intramolecular D-A integrated CN photocatalyst by doping m-aminophenylboronic acid (Wang et al., 2023, Zhou et al., 2022b). The optimized photocatalyst has a porous nano layered morphology, large specific surface area, superhydrophilicity, enhanced visible light utilization efficiency and carrier migration efficiency (Zhou et al., 2022b). The HER rate reached 1914 μmol $g^{-1}h^{-1}$ (5.9 times that of the original CN). 10 mg catalyst can degrade 81.3 % of high concentrations TC (40 mg/L) within 100 min.

2.2.2. S doping

The S element is abundant in the Earth, with small electronegativity and radius, making it easy to introduce into the CN framework, facilitating the migration of charges and effectively broadening the utilization range of CN for visible light (Sun et al., 2018a). In addition, as mentioned above, the doping of sulfur element can introduce lone pair electrons, which has great potential in regulating electronic structure and awakening n-π* electron transition of CN, and significantly expands the visible-light utilization (Zhang et al., 2017). Various S source, e.g., thiourea, thioacetamide, benzyl disulphide, H_2S and trithiocyanuric acid, were served as doping agents (Lv et al. 2020b).

Using a simple ternary self-assembly method, Fei et al. introduced trithiocyanuric acid as an additional component into melamine and cyanuric acid, and formed supramolecular intermediates through hydrogen bonding self-assembly, successfully introducing S into the skeleton of CN (Fei et al., 2021). After calcination, the morphology of the sample changed from spherical to peony like with a significant increase in specific surface area. In addition, the introduction of sulfur atoms reduced the band gap and suppressed the recombination of electrons and holes. The HER rate of the optimal sample reached 567.7 mmol h^{-1}, which was almost 53 times higher than that of pure CN obtained from melamine calcination. Using dicyandiamide as the precursor and thioacetamide as the functional reagent, Liu et al. prepared CN nanosheets doped with sulfur and functionalized with structural defects through copolymerization and thermal oxidation etching (Liu et al., 2021). The incorporation of methyl groups caused the formation of flaky defect structures in the sample, which, in conjunction with sulfur doping, enhanced the reducing ability of the sample and improved the light utilization and dissociation efficiency of excitons. The degradation rates of RhB and tetracycline hydrochloride by this material are 4.95 times and 2.07 times higher than those of single CN.

2.2.3. O doping

In contrast to S element, the O element possesses stronger electronegativity and also contains lone pair electrons. At the same time, the O atom can also be doped into the 3,s-triazine structure of CN by replacing the coordinating N atom. Via efficient and facile hydrogen peroxide-assisted hydrothermal reforming of melamine, Professor Sun fabricated a series of O-doped CN nanosheets with an enlarged CB edge for boosted HER activity (Sun et al., 2018b). Subsequently, they prepared hydroxylated and carbonylated melamine precursor and further designed a targeted porous O-doped CN nanosheets via thermal polymerization reaction (Song et al., 2019). Fu et al. constructed a porous CN

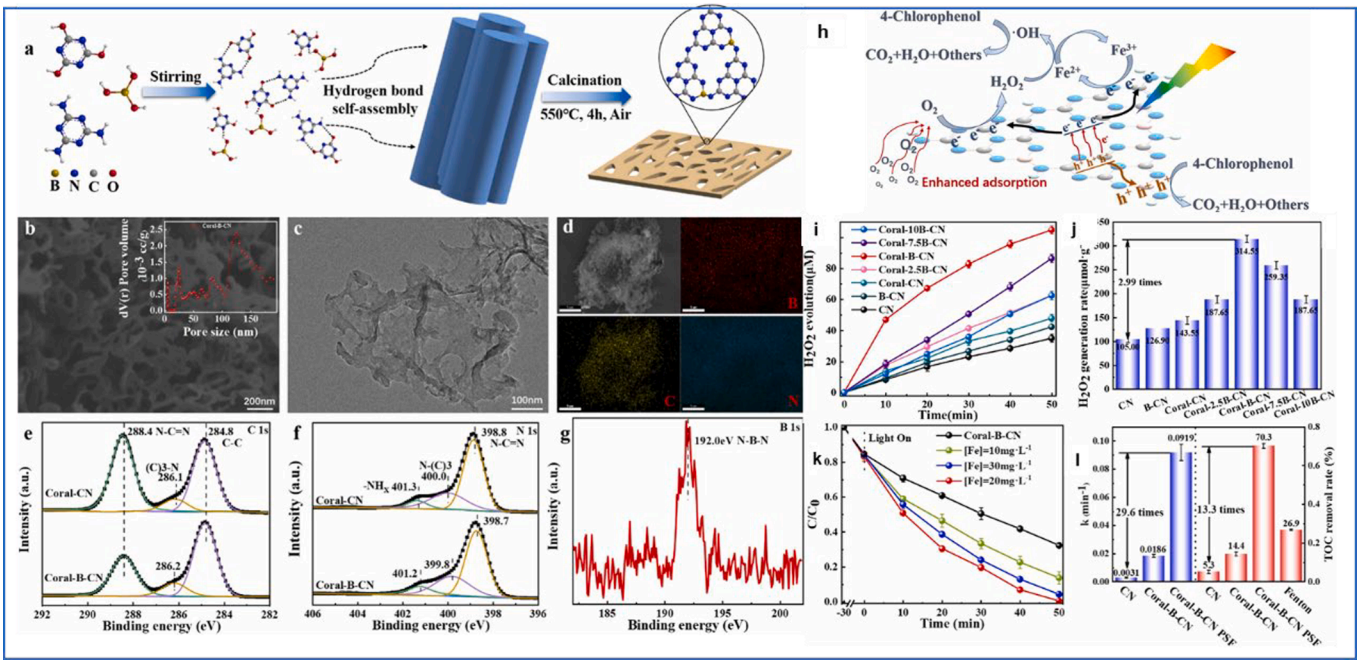

Fig. 8. Schematic illustration of Coral-B-CN synthesis (a); SEM (b), TEM (c) and EDS mapping (d) images of Coral-B-CN; C 1s (e) and N 1s (f) XPS spectra of Coral-B-CN and Coral-CN; B 1s XPS spectra of Coral-B-CN (g); Mechanism of photocatalysis-self-Fenton degradation of 4-CP via Coral-B-CN (h); H_2O_2 yield (i) and rate (j) curves for different catalysts; Adjustment of Fe concentration (k); k-value and TOC removal rate for different systems (l). Copyright 2023 Elsevier (Jing et al., 2023).

with a layered structure by continuously thermal oxidizing, exfoliating, and curling of bulk CN. This unique structure elevated the specific surface area of CN, exposed more active sites, and improved the utilization efficiency of visible light (Fu et al., 2017). The preparation process involved continuous high-temperature oxidation, where O atoms replaced nitrogen or carbon atoms, and were incorporated into layered porous CNs, optimizing the band structure, adjusting optical properties, and reducing the band gap of photogenerated carriers.

Unlike high-temperature calcination, Wang et al. synthesized O-doped CN catalysts at low temperatures using a simple one-pot solvothermal method. During the preparation process, O_2 molecules are activated and doped into the lattice of heptane heterocycles. As the prolong of condensation time, more and more O elements were doped, which promoted the reduction of band gap and enhanced the efficiency of charge dissociation, and the structure of CN was effectively regulated (Wang et al., 2017). Compared to the original CN prepared by high-temperature calcination, this material exhibited better visible light response and better photocatalytic performance in purifying environmental pollutants and producing hydrogen through water splitting. Employing H_2O_2 hydrothermal method for the first time, Li et al. doped O into CN (Li et al., 2012). The doping of O atoms regulated the intrinsic electron and band structure of the material, resulting in an elevated specific surface area and superior light utilization compared to pure CN. Under visible light, the degradation for methyl blue and HER performance were excellent.

2.2.4. C doping

C doped CN with abundant π-electron densities can be fabricated via the copolymerization of two different N-rich precursors with suitable physicochemical properties (Chen et al., 2018, Zhao et al., 2022). Yi' group fabricated a C doped CN through a hydrothermal-conjugate-copolymerization method, which signified that the rich C can regulate electronic structure and accelerated charge migration (Chen et al., 2018). Utilizing hydrogen bonds self-assembly of melamine and glucosamine-hydrochloride followed calcining, Zhao et al. constructed C doped CN microtubes with a large π-electron conjugated system (Zhao et al., 2022). The tubular morphology and π-delocalization electron caused by C doping beneficial to charges migration, broaden more active sites and enhance visible-light availability. The C-doped CN microtubes revealed a superior HER rate of 3888.9 μmol h^{-1} g^{-1}, far beyond that of single CN. The group of Professor Jiang designed a C-doped 1D thin porous strip-like CN with large π delocalization, and realized simultaneous regulation of morphology and electronic structure (Li et al., 2021b). Dopant of nicotinic acid, bearing carboxyl group and pyridine ring, assembled with melamine and obtained the strip-like supramolecular precursor via hydrogen bond under hydrothermal process. After calcination of the precursor, the 1D thin porous strip-like CN with effective π delocalization was obtained, and the carbon-doping and porous structure accelerated mass/charge/carrier transfer and supplied more active sites.

2.2.5. Cl doping

In recent years, Cl has also been proven to be a suitable element for modifying CN due to its moderate electronegativity that can regulate the electronic structure of CN and enhance oxygen adsorption (Aleksandrzak et al., 2021a, Li et al., 2022c, Liu et al., 2022b). Furthermore, Cl doping can form p-π conjugation with CN, effectively regulating the electronic structure of CN and improving its photocatalytic performance. Liu et al. prepared Cl doped g-C_3N_4 by thermal-pyrolysis of melamine and excess ammonium chloride. The insertion of Cl element into the interlayer structure of CN given CN a uniformly porous characteristic, and the established interlayer structure, which significantly promoted electron migration, making the level of CB more negative and rising the specific surface area (Liu et al., 2017). The doped sample suppressed the recombination of carriers, diminished the bandgap, and increased the number of reaction sites. Compared with the original CN, the hydrogen production performance had been improved by 19.2 times. At 420 ± 15 nm, the AQE reached 11.9 %, and the photo oxidation and photo reduction abilities were significantly enhanced. Aleksandrzak et al. successfully synthesized Cl doped CN nanosheets using the condensation method. The research has found that Cl atoms were not inserted into their π-conjugated plane, but rather in the middle layer of CN. Compared with the original CN, the HER efficiency was increased by 4.4 times (Aleksandrzak et al., 2021b).

Through a simple solvothermal synthesis method, Li et al. introduced Cl element into the CN framework (Zhang et al., 2022d). The doping of Cl element effectively improved the migration rate of charges, regulated the band gap, and reduced the activation energy of oxygen reduction reaction. The experiment showed that the production rate of H_2O_2 in the doped sample under visible light was 1.19 ± 0.06 μM min^{-1}, which was 104 times higher than the original CN. In addition, using isopropanol as a hole scavenger can effectively inhibit the separation of photogenerated excitons, decrease the decomposition of H_2O_2 and photocorrosion. Under the presence of a scavenger, the continuous net production of H_2O_2 was 2.78 ± 0.10 μM min^{-1} and could last for 54 h, which was much higher than the condition without scavenger. It is signified that the doping of Cl element effectively boosted the activity of CN.

2.2.6. P doping

Another widely studied non-metallic element doped to modify CN is P element, due to its well-matched sp^3d hybridization in the planar structure of heptazine units in contrast to other non-metals (Mahvelati-Shamsabadi and Lee, 2020, Yu et al., 2022). Generally, the P atom supplies an electron-rich circumstance due to its five valence electrons that merge into melon units in contrast to carbon (four valence electrons). The one extra electron of P atom in contrast to carbon enhances conductivity of CN and the mobility of charges, thus boosting the photocatalytic activity (Mahvelati-Shamsabadi and Lee, 2020, Yu et al., 2022). Li et al. constructed ultra-thin porous P-doped CN nanosheets using one-step thermal polymerization method. The doping of P changed the molecular structure of CN, altered local electronic structure, reduced band gap, and improved the utilization efficiency of visible light (Che et al., 2022, Yang et al., 2022). Meanwhile, due to the low work function of P-doped sites, electrons were readily migrated to small molecular, raising electron hole dissociation and promoting the reduction reaction of O_2. The optimized photocatalyst can produce 285.34μ M of H_2O_2 within 3 h (3.41 times that of the original CN), and the rate constant of photodegradation diclofenac was 46.22 times that of the original CN.

Fang et al. fabricated a fragmented P-doped CN nanoflakes via a facile doping and post-treatment processing, where biomass raw material phytic acid was served as P source to calcinate with urea (Fang et al., 2018). The obtained material revealed narrowed sub-bandgap from VB to intermediate states, broadened light-absorption toward 800 nm, and increased the surface area to 223.2 m^2/g. The fragmented nanoflakes structure created a significantly shortened migration distance of charge-to-surface in both vertical and planar directions. Benefiting to the integration effect of P doping and fragmented nanosheets structure, the material presented a prominent HER rate of 15921 μmol h^{-1} g^{-1} (>420 nm), 9546 μmol h^{-1} g^{-1} (>470 nm) and AQE (6.74 % at 420 nm and 0.24 % at 600 nm).

Integrating thermal exfoliation techniques with element doping, Deng et al. fabricated P-doped ultrathin porous CN nanoflakes with highly stable chemical properties (Deng et al., 2017). The crystal structure of the prepared catalyst was regular due to large number of in-plane pores, which raised the number of active sites compared to the original CN. The doping of P broadened the response range of visible light, suppressed the recombination of carriers, and greatly elevated the electron transfer efficiency. The synthesized material has strong photocatalytic activity and can simultaneously reduce Cr^{6+} and oxidize 2,4-dichlorophenol under certain dissolved oxygen and low pH conditions.

Generally, the electronegativities and reactivity of non-metals are

consistently high, enabling them to predominantly form covalent bonds through electron gain during synthetic reactions, where oxygen and chlorine elements with strong electronegativity, boron elements with electron deficiency, and sulfur and phosphorus elements with lone electron pairs (Jiang et al., 2017). Various researches have proved the effectivity of element doping in boosting photocatalytic activity of CN because element doping can adjust the electronic structure and light absorption region of CN. Despite various doping strategies and diverase small molecules were adopted, investigating controllable especially precise control over the molecular and crystal structures of CN with well-recognized dopants has always been pursuing.

2.3. Defects

Confined boundaries and serious interlayer aggregation often limit the exposure of catalytic active sites and charge transfer kinetics (Sun et al., 2019a). In this situation, defects in CN play an important role in sites exposure, catalytic kinetics, energetics and mechanism (Zhang et al., 2022a). According to the dimensionality, the various defects that can be induced in a semiconductor photocatalyst, such as 0D point defects, 1D line defects, 2D planar defects and volume defects (Kumar et al., 2021, Zhang et al., 2022a). Generally, Volume defects often control morphology or porosity, as well as adjust electronic/atomic structure of CN, which regulate specific surface area, pore volume, physicochemical stability, and surface functional feature, thus revealing the microstructure-property-performance relationship of CN (Song et al., 2021, Sun and Liang, 2017, Yang et al., 2024). 0D point defects can readily acquire in a semiconductor photocatalyst without significantly changing its structural makeup. Furthermore, different from line or planar defects, which barely affect stoichiometry, point defects serve to increase the conductivity of the photocatalyst by regulating the non-stoichiometric components (Kumar et al., 2021, Zhang et al., 2022a). Defects in this section discuss the situation where defects create from small molecules doping.

2.3.1. C defect

Doping CN with small molecules to form carbon defects can regulate its photocatalytic performance, which is a significantly effective and common method, because carbon vacancies act as charges acceptors to capture e^-, suppressing the recombination of photogenerated carrier (Shen et al., 2021). Huang et al. prepared four types of CN materials under four different environmental conditions, i.e., dry argon, humid argon, dry air, and humid air (Huang et al., 2021). The photocatalytic activity of samples prepared in humid environments was better than those synthesized under dry conditions, which was caused by the carbon defects generated. In humid environments, the presence of water molecules diminished the interlayer van der Waals forces of CN, and the presence of carbon vacancies increased band energy. The terminal amino groups on the material can preferentially dock with Pt co-catalysts, promoting carrier migration and electron transfer.

Via secondary calcination of bulk CN, Di et al. fabricate an ultra-thin porous CN with carbon defects (Di et al., 2016). The average thickness of the sample was 0.9 nm with plentiful pores distributed on the surface generated by carbon defects, which significantly raised the specific surface area. Due to the ultra-thin structure of the sample, the time for carrier transfer from the interior to the surface was shortened, which accelerated the migration of internal charges within the structure. The $\bullet O_2^-$ and •OH devoted strong photodegradation activity for RhB.

Wang et al. used formaldehyde as a carbon defect inducer and prepared g-C_3N_4 with carbon defect and oxygen doped by one-step formaldehyde-assisted thermal polycondensation of molten urea (Wang et al., 2021a). By precisely controlling the dosage of formaldehyde at a sufficiently small scale, the concentration of carbon defects in CN can be regulated, while the incorporation of oxygen atoms into the CN framework is attributed to molten urea rather than formaldehyde. The combination of carbon defects and oxygen doping not only leaded to a porous nanosheet structure of the sample, increasing the specific surface area and exposing abundant active sites, but also controlled the migration rate of charge carriers, generating more active oxygen species, which was more conducive to the degradation of pollutants.

2.3.2. N Defect

The generation of N vacancies in the CN framework through small molecule doping can also regulate the electronic structure and optical characters of CN, improve the dissociation efficiency of excitons, and further enhance photocatalytic performance (Shi et al., 2023, Yang et al., 2023). Through solid-state copolymerization and thermal annealing, Luo et al. prepared porous bridging nitrogen deficient CN nanosheets using melamine and hexamethylenetetramine as raw materials (Luo et al., 2021). The hexamethylenetetramine doped CN had a unique layered structure and a large number of voids, which dramatically hoisted the specific surface area and the amounts of active sites. The introduction of nitrogen defects promoted the separation rate of photogenerated exciton, inhibited carrier recombination, and greatly raised the light utilization. The optimized CN exhibited a HER rate of 2497.1 μ $molg^{-1}h^{-1}$ and AQY of 3.24 % at 420 ± 10 nm.

Through a low-temperature oxidation technique, Zeng et al. constructed a N vacancy and O substitution CN (Zeng et al., 2023). As time passed, the thermal oxidation CN flakes coiled into a hierarchical sphere-like CN after self-assembling into CN aggregations. The resulting N vacancy and O substitution CN revealed boosted degradation performances for TC, ciprofloxacin and sulfadiazine, and the first-order kinetic constants were 2.10, 2.24 and 1.38 folds higher than those of CN.

Cheng et al. employed directly thermal polymerization to prepare porous nitrogen deficient CN using allophanamide as a precursor (Cheng et al., 2021). The synthesized sample contained plentiful nitrogen defects and remote atomic disordered structures, which regulated the band structure of the sample, improved the dissociation of photoproduced exciton and increased the utilization of visible light. A large number of voids raised the specific surface area of the sample, and the active sites of the light absorption reaction were also increased. The experimental results demonstrated that the synthesized sample has excellent photocatalytic H_2 and O_2 production capabilities with an AQY of 45.5 % at 420 nm.

Shen et al. prepared nitrogen deficient CN nanosheets using a calcination solvent-thermal calcination method (Shen et al., 2020). Due to the introduction of nitrogen defects in the doping of 2,5,8-triamino-tris-s-triazine, the sample presented a fragmented few layer nanostructure with an increased specific surface area, shortened the migration distance of photogenerated charges, adjusted the redox potential and abundant reactive sites. Under the action of visible-light, the HER rate of the sample reached 5375 μmol $h^{-1}g^{-1}$, which is 33 times that of original CN. The research provided a new approach for achieving efficient photocatalytic hydrogen production.

Defect engineering modification can enhance the catalytic activity of CN and has been extensively applied in various photocatalytic systems. However, the enhancement in activity of CN with a single defect is not significant. Integrating defect sites with element doping or special functional groups are gradually being attempted.

Utilizing a dual strategy of modifying succinic acid and solvent dispersion, Huo et al. fabricated porous CN nanotubes with carbon and defect (nitrogen vacancy) (Huo et al., 2021). Compared with the block CN sample, the porous CN nanotubes exhibited a larger specific surface area and improved light utilization effect. The synergism of carbon and defect (nitrogen vacancy) adjusted the band gap structure, accelerated the rate of charge separation and hydrogen evolution. Using triethanolamine and bisphenol A as electron donors separately, the HER rates of the synthesized samples were 13 times and 84 times higher than those of PCN, and the bisphenol A can be directly oxidized by hole to achieve simultaneous degradation and mineralization.

Similarly, employing ammonium persulfate to oxidize CN, Lin et al. prepared oxygen doped CN (Lin et al., 2021b). Then, the sample was

calcined in a hydrogen environment to prepare CN with both oxygen and nitrogen defects. Due to the stronger electronegativity of oxygen compared to nitrogen, oxygen would be preferentially reduced during hydrogen reduction process, which is beneficial for the generation of oxygen defects. The dual defects jointly adjusted the band structure of CN, causing the upshift of CB position, increasing the specific surface area, and restraining the recombination of photoproduced carriers. The HER rate of the optimized sample was 11.7 times and 5.8 times higher than that of CN and O-doped CN.

Integrating defect sites with special functional groups, Zhang et al. prepared a photocatalyst with dual defect sites by introducing −C≡N groups and N defects into the CN framework through a two-step reaction (Zhang et al., 2022d). The generation of double defects changed the electronic structure of CN, and the synthesized sample presented a unique electron rich structure, promoting the migration of photogenerated carriers, forming higher selectivity reaction sites, and greatly enhancing light absorption ability. The N defects effectively adsorbed and activated O_2, and −C≡N effectively adsorbed H^+, which synergistically promoted the generation of H_2O_2. The rate of photocatalytic production H_2O_2 in the optimized sample was 3093 μmol $g^{-1}h^{-1}$, and the AQE at 400 nm reached 36.2 %.

Much effort has been made to boost the activity of CN through doping small molecule to control defects. By adopting a reasonable defect engineering strategy, CN with defects can better regulate its band structure, expand the light absorption range, and propel the photocatalytic activity. Meanwhile, vacancies in defects can serve as capture and adsorption sites, promoting the separation and transfer of charge carriers, and improving the adsorption capacity of CN for reaction molecules (Cheng et al., 2021, Di et al., 2016, Guo et al., 2019, Huang et al., 2021, Luo et al., 2021, Shen et al., 2020, Wang et al., 2021a). Currently, the characterization and proof methods for defects relatively limite mainly involving elemental analysis, XPS, solid-state NMR of carbon/nitrogen spectroscopy and electron spin resonance, etc (Yang et al., 2024). In the future, the more powerful characterization testing methods will be emphasized and development.

3. Challenges and future prospects

Through the continuous exploration of researchers, the performance of CN materials doped with small molecules has been greatly improving (Table 1 and Table 2). Although research on CN based materials is relatively extensive, there are still some challenges (Fig. 9).

3.1. Preparation process

Firstly, most of the preparation methods for propelling the catalytic activity of CN based on small molecule doping are based on high-temperature calcination of nitrogen-rich substances and small molecule, or high-temperature calcination of hydrothermal precursor pre-synthesized with nitrogen-rich substances and small molecules (Tong et al., 2022). The relevant reaction mechanisms and control methods for "whether small molecules can maintain their intrinsic characteristics under high temperature conditions or participate in CN skeleton composition?" need to be clarified. Professor Sun reported creatinine-derived moiety as donor block for CN with improved absorption and optimized charge behavior, where the matrix-assisted laser desorption ionization-time of flight mass spectroscopy was employed to reveal the N-rich species generated during the condensation (Zong et al., 2021). Combined the theoretical calculation (HOMO distributes at the creatinine-derived moiety unit and LUMO distributes the melem unit), first disclosed the condensation process of creatinine and urea.

Secondly, in common preparation processes, urea was first decomposed into cyanic acid and isocyanic acid, followed by generated biuret and cyanuric acid. After forming melamine, melem can be obtained, which further extends to produce CN frame along the edge amino groups (Chen et al., 2020c, Zhou et al., 2018). In most studies, doping extremely little amounts of small molecules (<0.5 % wt.) can achieve a significant improvement in catalytic performances. How can such a low content of small molecules participate in the condensation process of urea and significantly improve the catalytic performance of the product? Which stage does small molecules participate in urea condensation? It is not clear which intermediate it reacts with small molecules. It is difficult to fundamentally explain the above issues solely through the structural characterization and performance comparison of the products. Therefore, more reliable proof technologies like in situ characterizations need to be developed in the future to elucidate the reaction mechanism.

Thirdly, there are plentiful strategies on significantly improving the photocatalytic activity of CN through small molecule doping, but there are few reports detailing its yield. Based on the years of research experiences, the yield of CN synthesis is not satisfactory, which seriously limits the potential of CN in large-scale production applications. During the preparation process of CN, urea can undergo decomposition to generate plentiful NH_3 and CO_2, which function as the N-source supplier and the template for bubble generation, respectively (Wang and Yang, 2017). Excessive NH_3 escape can result in a decrease in production, and a common solution is to cover the perforated tin foil. Yang et al. reported a high-yield CN through in-situ direct pyrolysis of cyanamide assisted by bifunctional urea (Wang and Yang, 2017), where the dissolution of the urea into molten cyanamide at 60 ∘C lead to the formation of an intermolecular hydrogen bonds network. This hydrogen bonds network effectively suppresses NH_3 escape, resulting in a high CN yield of 60–70 %. Furthermore, appropriate reaction time and temperature can enhance the yield and purity of CN, while avoiding insufficient reaction and excessive impurities. Meanwhile, synthesis in a N_2 or Ar atmosphere can effectively prevent oxidation of CN.

3.2. Characterizations and theoretical calculations

Most of the current research on CN based materials is still in the stage of fundamental research, and the elucidation of the reaction mechanisms related to synthesis and catalytic applications is not accurate enough. Generally (Fig. 2), SEM, HRTEM, AFM and BET etc., were first conducted to obtained the basic morphology, then XRD, FTIR, XPS, raman and Solid-state ^{13}C NMR etc., tests were employed to confirm basic structure, following the optoelectronic analysis (e.g., photocurrent, impedance, PL, TRPL) to signify the charge transfer properties. After optimizing and evaluating the photocatalytic performances, theoretical calculations combined with free radical exploration are used to explain the photocatalytic mechanism. Currently and in the future, more and more novel and reliable characterization methods (such as X-ray absorption near edge structure, in-situ XPS/Raman/infrared, etc.) integrating powerful experiments phenomenon were employed to clarify the influence of the structure/defects/charge behavior of CN-based materials on catalytic mechanisms.

In terms of theoretical calculations, most studies speculate on the structure of CN doped with small molecules through a series of characterizations, in which form CN skeleton, element doping or form defects were pre-confirmation. Subsequently, the confirmed structure was optimized via DFT theoretical calculations to obtain its HOMO/LUMO levels, dipole moment, Barder charge, APT charge, electrostatic potential, density of states, etc (Che et al., 2023a). Recently, our group fabricated a fragmented intramolecular D-A integrated CN (FBCN) through thermal-melting m-aminophenylboronic acid and urea followed two-step post-processing (Wang et al., 2023). The deformation of electron density, raised dipole moment and redistributed HOMO-LUMO via DFT theoretical calculations manifest the formation of D-A integrated structure and the rise of intramolecular polarity, which strengthen driving power for exciton dissociation and carrier migration driving forces, thus significantly boosting photocatalytic activity. However, the common theoretical calculation is based on the fragments structure of CN, while according to the previous analysis, the doping dosage is extremely low, let alone the proportion of this fragment in the entire

Table 1
Comparison of photocatalysis clean energy production performance of small molecule doped CN reported in recent years.

Designing strategy	Photocatalysts preparation	Condition	HER Performance, improvement times, AQE	CocatalystsSacrificial reagents	Ref.
Ultrathin porous CN nanocages via host–guest supramolecular self-assembly	Calcining melamine, oxamide, cyanuric acid and urea	300 W Xe lamp	1135 μmol h^{-1} g^{-1}	10 vol% TEOA 2 wt% Pt	(Tong et al., 2022)
Forming local micro-π conjugate connection units in the structure of CN composites	Acid-base reaction between trimesic acid and melamine	300 W Xe lamp with a 420 nm cutoff filter	301 μmol $g^{-1}h^{-1}$,21.8 times	10 vol% TEOA 3 wt% Pt	(Yuan et al., 2021)
Asymmetric embedded benzene ring enhances CN	Dicyandiamide mixed calcination with terephthalonitrile followed second annealing process	300 W Xe lamp with a 420 nm cutoff filter	11.3 % at 400 nm and 9 % at 420 nm. 10.8 times	10 vol% TEOA 3 wt% Pt	(Jia et al., 2019)
Increasing π-electron availability in benzene ring incorporated CN	Calcining supramolecular mixture of melamine and trimesic acid	300 W Xe lamp with a cut-off filter (>420 nm)	3.4 times enhancement	10 vol% TEOA 0.5 wt% Pt	(Lin et al., 2021a)
Boron doped intramolecular donor–acceptor integrated CN	One-pot thermal copolymerization of small molecule precursor (m-aminophenylboronic acid, m-aminophenol or aniline) with urea	300 W Xe lamp with a cut-off filter (>420 nm)	1914 μmol $g^{-1}h^{-1}$, 5.9 times	10 vol% TEOA 3 wt% Pt	(Zhou et al., 2022b)
Phenyl-bridged CN with a porous and hollow sphere structure	Calcining supramolecular mixture of cyanuric acid, trimesic acid and melamine	λ ≥ 420 nm	4.455 mmol $g^{-1}h^{-1}$, 48.42 times	10 vol% TEOA 3 wt% Pt	(Chen et al., 2020b)
CN with the dual defect sites, i.e., –CN groups and N vacancies	Calcining urea and thiourea followed calcining C≡N-CN in a tube furnace under argon	300 W Xe lamp with 420 nm cutoff film (λ ≥ 420 nm)	H_2O_2 generation rate of 3093 μmol $g^{-1}h^{-1}$, AQE of 36.2 % at 400 nm	10 % isopropanol	(Zhang et al., 2022d)
Defects controlling, elements doping and crystallinity improving triple-strategy modified CN	Calcining melamine and cyanuric acid followed thermal post-treatment with sodium cyanoborohydride	Xe lamp (300 W, λ > 420 nm	620 μmol $g^{-1}h^{-1}$ of H_2O_2 (309 μmol $g^{-1}h^{-1}$)	10 vol% ethanol (or without sacrificial agents)	(You et al., 2023)
Carbon doped CN microtubes with a large π-electron conjugated system	Hydrogen bonds self-assembly of melamine and glucosamine hydrochloride followed calcining	300 W Xe lamp with a 400 nm cut filter	3888.9 μmol $g^{-1}h^{-1}$	10 vol% TEOA −wt% Pt	(Zhao et al., 2022)
Ultrathin porous phosphorus-doped bifunctional CN nanosheet	Calcining dicyandiamide, NH_4Cl and 1-Hydroxyethylidene-1,1-diphosphonic acid	9 W blue LED lamp with λ in 410–530 nm	285.34 μM of H_2O_2, 3.41 times	10 vol% ethanol	(Wang et al., 2022b)
One-dimensional P-doped CN tube	Hydrothermal reaction of melamine and $Na_2HPO_4{\cdot}12H_2O$ followed calcination under N_2 atmosphere	300 W Xenon lamp with a 420 nm cut-off filter	2749.3 μmol $g^{-1}h^{-1}$, 17.5 and 6.6 times higher than that of the bulk CN and CN tube	20 vol% TEOA 1 wt% Pt	(Yu et al., 2022)
Sulfur-doped 2D CN nanosheets	Thermal polycondensation of the thiourea	Xe lamp with an output power of 140 W	127.4 μmol h^{-1}, AQE 8.35 % at 420 nm	5 vol% TEOA 1 wt% Pt	(Lv et al. 2020a)
Self-assembled sulphur doped CN	Calcination of thiosemicarbazide at different temperature	300 W Xe lamp	14.7 mmol $g^{-1}h^{-1}$ from water/methanol over 95 h without CO evolution, AQE of 30 % at 365 nm	Methanol solution (0 %-100 %) 1 wt% Pt	(Wang et al., 2022a)
3D peony-like sulfur-doped CN	Calcinating melamine, cyanuric acid and different masses of trithiocyanuric acid	300 W Xe lamp with a 400 nm cut-off filter	567.7 mmol h^{-1}, 53 times	10 vol% TEOA 3 wt% Pt	(Fei et al., 2021)
Chlorine-doped CN nanostrips	Calcinating melamine and terephthalonitrile	300 W Xenon lamp with a 420 nm cutoff filter	76 mmol h^{-1} g^{-1}, 16.5 times, AQY of 8.91 % at 420 nm	TEOA	(Peng et al., 2021)
Chlorine-doped CN	Solvothermal method cyanuric chloride and melamine	1000 W Xe lamp with a water optical filter to remove IR light	1.19 ± 0.06 μM min^{-1} of H_2O_2, 104 times	10 vol% isopropanol	(Li et al., 2022c)
Chlorine doped CN nanodisc	Calcination of melamine followed one step HCl treatment	–	241.3 mmol $g^{-1}h^{-1}$, 4 folds, (RhB 98 % 60 min, 2.18 folds)	TEOA without Co-catalyst	(Liu et al., 2022b)
Ionic liquid-assisted synthesis of porous boron-doped CN	Evaporation the mixture of $[Emin]BF_4$ and urea followed calcination	350 W Xe lamp with a light cut-off filter (>365 nm)	901 mmol $g^{-1}h^{-1}$, almost 3 times	12.5 vol% TEOA	(Qi et al., 2021)
1D strip-like porous CN	Nicotinic acid and melamine assembled the strip-like supramolecular via hydrogen bond under hydrothermal process followed calcination	300 W Xenon lamp (λ > 420 nm)	126.2 μmol h^{-1}, about 18 folds, AQE is 6.81 % at 420 nm	10 vol% TEOA 1 wt% Pt	(Li et al., 2021b)
Pyridine ringsgrafted on CN edge	Calcinating urea and 2-aminopyridine	300 W Xe lamp with a 420 nm cut-off filter	6317.5 μmol $g^{-1}h^{-1}$ 3.9 folds, AQE is 20.1 % at 420 nm	20 vol% TEOA 3 wt% Pt	(Li et al., 2021a)
Limbic inducted and delocalized effects of diazole in CN skeleton	Calcination of urea with 4-aminoantipyrine	300 W Xe lamp with a 420 nm cutoff filter	284.2 μmol h^{-1}, 10 times, AQE is 24.2 % at 420 nm	10 vol% TEOA 3 wt% Pt	(Dong et al., 2021b)
Polymeric CN with donor-π-acceptor network	Calcination of urea wit π-aromatic 2,3-diaminopyridine	LED lamps (60000–65000 lx)	6.56 mmol $g^{-1}h^{-1}$, 4.5 times	10 vol% TEOA 2 wt% Pt	(Bhoyar et al., 2022)
Intramolecular π-conjugated channel expansion achieved by doping cross-linked dopants into CN frameworks	Calcination of dried urea and pyrimethamine	300 W Xe lamp with a 420 nm cutoff filter	5.418 mmol $g^{-1}h^{-1}$, 11.6 times. AQE is 17.7 % at 420 nm	10 vol% TEOA 3 wt% Pt	(Zhang et al., 2022c)

(*continued on next page*)

Table 1 (*continued*)

Designing strategy	Photocatalysts preparation	Condition	HER Performance, improvement times, AQE	CocatalystsSacrificial reagents	Ref.
Boron/Oxygen-co doped CN nanomesh	Thermal polymerization of melamine followed second calcination. Soaking in saturated H_3BO_3 solution followed freeze-drying and calcinating under N_2	300 W Xe lamp with a cut-off filter ($\lambda \geq 420$ nm	9751 μmol $g^{-1}h^{-1}$, 28 times	10 vol% TEOA 3 wt% Pt	(Du et al., 2021)
Donor-π-Acceptor-π–Donor structured CN	Calcination of dried urea and 4,4′-(benzoc 1,2,5 thiadiazole-4,7-diyl) dianiline	300 W Xe lamp with a cut-off filter ($\lambda \geq 420$ nm	3428 μmol $g^{-1}h^{-1}$, nearly 6 times	10 vol% TEOA 3 wt% Pt	(Li and Zhang, 2018)
Carbon self-doped CN hexagonal tubes	Facile in situ solvothermal method with melamine and glucose as precursor and additive	300 W Xe lamp ($\lambda >$ 420 nm)	32.3 μmol h^{-1}, $\lambda >$ 420 nm, 4.24 and 12 folds	10 vol% TEOA 3 wt% Pt	(Yang et al., 2019)
Ultrathin porous carbon nitride bundles with an adjustable energy band structure	The pyrolysis of an asymmetric supramolecular precursor prepared from L-arginine and melamine	300 W Xe lamp with AM1.5 transmission filter at current strength of 15 Å	95.3 mmol h^{-1} and meanwhile phenylcarbinol was selectively oxidized to benzaldehyde (conversion of 90.9 %, selectivity of 99.7 %)	–	(Wu et al., 2021a)
Foamer-derived bulk nitrogen defects and oxygen-doped porous CN	Thermal polymerization of urea with the foaming agent azoformamide or azodicarbonamide	LED light source of 420–425 nm	44.7 μmol h^{-1} and the oxidation of diphenylhydrazine to azobenzene with conversion and selectivity of almost 100 %	–	(Wang et al., 2021b)
Tubular CN S-schemehomojunctions	One-step pyrolyzing urea and L-cysteine	$\lambda >$ 420 nm	4548.4 μmol $g^{-1}h^{-1}$, 35 folds improvement	10 vol% TEOA 1 wt% Pt	(Ma et al., 2021)
Bridging-nitrogen defects modified CN	Pyrolyzing melamine and hexamethylenetetramine	300 W Xe lamp, $\lambda >$ 420 nm	2497.1 μmol $g^{-1}h^{-1}$, 10.4 and 41.1 folds improvement	10 vol% TEOA 3 wt% Pt	(Luo et al., 2021)
Disordered nitrogen-defect-rich porous	Calcination of biuret, urea, thiourea, dicyandiamide, and melamine	300 W Xe lamp, $\lambda >$ 420 nm	19583 μmol $g^{-1}h^{-1}$, 45.5 % at 420 nm	10 vol% TEOA 3 wt% Pt	(Cheng et al., 2021)
CN with n-π* electronic transition for extending light absorption and reducing charge recombination	Thermolyzing the supramolecular aggregates of dicyandiamide via a microwave-assisted heating route	300 W Xe lamp	5553 μmol $g^{-1}h^{-1}$, 12 times	10 vol% TEOA 0.5 wt% Pt	(Zhao et al., 2023)
Intramolecular charge transfer and extended conjugate effects in donor-π-acceptor-type mesoporous	One-pot thermo polymerization based on nucleophilic substitution and a Schiff-base chemical reaction with urea and 4-iodobenzaldehyde	300 W Xe lamp, $\lambda >$ 420 nm	3882.09 μmol $g^{-1}h^{-1}$, 12 times	17 vol% TEOA 3 wt% Pt	(Sun et al., 2019b)
D-A integrated CN	Copolymerization of urea and 5,8-DibroMoquinoxaline	300 W Xe lamp, 400 $< \lambda <$ 800 nm	3012.5 μmol $g^{-1}h^{-1}$, 3.3 times, 1.3 % at 420 nm	10 vol% TEOA 2 wt% Pt	(Wan et al., 2022)
Creatinine-derived moiety as donor block for CN photocatalyst	Copolymerization of creatinine and urea	300 W Xe lamp, $\lambda >$ 420 nm	9454 μmol $g^{-1}h^{-1}$, 420 nm 8.41 %, 500 nm 4.57 %.	10 vol% TEOA 1 wt% Pt	(Zong et al., 2021)
CN with push–pull system	Calcination of acetylacetone with urea	300 W Xe lamp, $\lambda >$ 420 nm	18.8 % at 450 nm	10 vol% TEOA 3 wt% Pt	(Xu et al., 2020)
Nitrogen doped carbon ribbons modified CN	Calcination of urea and formaldehyde resin	300 W Xe arclamp with different λ	84.32 μmol h^{-1}, 54.75 and 6.51 times higher than that of calcination of melamine or urea	20 vol% TEOA 3 wt% Pt	(Che et al., 2020)
Donor-acceptor system on CN nanosheets	Calcination of cyanuric acid, urea and 150 phenylurea	300 W Xe lamp, $\lambda >$ 420 nm	7.394 mmol $g^{-1}h^{-1}$, 7.67 times	10 vol% TEOA 3 wt% Pt	(Chen et al., 2021a)
Edge donor–acceptor integrated CN	Calcination of m-aminophenylboronic acid and urea	300 W Xe lamp, $\lambda >$ 420 nm	1914.3 μmol $g^{-1}h^{-1}$	10 vol% TEOA 3 wt% Pt	(Zhou et al., 2022b)

material. Therefore, to improve the soundness of CN in theoretical calculations, the more accurate structural confirmation combined with actual macroscopic test to assist theoretical calculations and explain the mechanism is crucial.

After optimizing the material structure, the adsorption energy of the material for hydrogen, oxygen or PMS were further calculated, and the adsorption sites were confirmed. Through the calculation of pollutant Hirshfeld charges, vulnerable sites were searched, where pollutants are easily attacked by free radicals. Combining the main active species tested by the radicals capture experiments and ESR tests, the pollutant removal mechanism was clarified. Combining high-performance liquid chromatography tandem mass spectrometry to obtain degradation intermediates, intermediate toxicity and pathways, the actual applicability was evaluated.

3.3. *Efficiency and application*

With the expansion of research scale and deepening of research, the catalytic performance of CN has repeatedly reached new heights.

In the aspect of clean energy production, most of the reported HER systems based on CN materials require plentiful sacrificial agents and cocatalyst (Table 1), which increased costs and environmental risks. Moreover, the HER in water splitting systems is still far from the optimal level of practical application, especially for industrialized application. In the future, an increasing number of CNs that do not require sacrificial agents or cocatalysts will pursued for sustainable industrial application. Some novel method like plasmon-enhanced strategy, molecular dynamics simulations and structure-modal analysis will be adopted (Fakhrabadi et al., 2013, Ghaderi et al., 2021, Khani et al., 2014). The plasmonic nanostructures and their optical properties are able to prohibit the recombination of charge carriers and promote the absorption

Table 2
Comparison of photodegradation performance of small molecule doped CN reported in recent years.

Designing strategy	Photocatalysts preparation	Condition	DegradationEfficiency, TOC removal rate	Catalysis timeVolume	Pollutant concentrationCatalyst dosage	Ref.
Donor-acceptor structured g-C_3N_4	Calcination 5-bromo-2-thiophenecarboxaldehyde with urea	300 W Xe lamp with a cut-off filter (>420 nm)	93 % oxytetracycline TOC 38 %	60 min 100 mL	50 mg/L 20 mg	(Zhang et al., 2022a)
Boron doped intramolecular D-A integrated CN	One-pot thermal copolymerization of m-aminophenylboronic acid, m-aminophenol or aniline with urea	300 W Xe lamp with a cut-off filter (>420 nm)	81.3 % TC	100 min 50 mL	40 mg/L 10 mg	(Zhou et al., 2022b)
Fragmented intramolecular D-A integrated CN	Calcination of m-aminophenylboronic acid doping followed two-step post-processing	300 W Xe lamp with a cut-off filter (>420 nm)	87 % sulfamethoxazole, 3.9 times	100 min 50 mL	10 mg/L 10 mg	(Wang et al., 2023)
Benzene ring modified CN	Calcination of dicyandiamide and diphenylcarbazide	300 W Xe lamp with a 420 nm cutoff filter	72 % oxytetracycline, 2.1 times	60 min 100 mL	10 mg/L 15 mg	(Dong et al., 2022b)
Ultrathin porous phosphorus-doped bifunctional CN nanosheet	Calcination of dicyandiamide, NH_4Cl, and 1-Hydroxyethylidene-1,1-diphosphonic acid	9 W blue LED lamp with λ in 410–530 nm	99.4 % diclofenac, 46.22 times	100 min 50 mL	20 mg/L 10 mg	(Wang et al., 2022b)
Sulfur-doped 2D CN Nanosheets	Thermal polycondensation of the thiourea	300 W Xe lamp	93 % phenol	90 min 100 mL	50 mg/L 10 mg	(Lv et al. 2020b)
Sulfur doping and structure defect functionalized CN nanosheets	Direct copolymerization of dicyandiamide and thioacetamide	300 W Xe lamp	93.06 % RhB	120 min 30 mL	12 mg/L 20 mg	(Liu et al., 2021)
Internal electric field construction on dual oxygen group-doped CN	Two-step thermal treatment process of urea and CH_3COONH_4	Xe light (λ > 420 nm)	Bisphenol A, 2-chlorpheno and diphenhydramine 96.7 %, 97.3 % and 88.6 %. TOC 67.3 %, 61.5 % and 55 % within 60 min.	30 min – mL	10 mg/L – mg	(Li et al., 2019)
Advancing n-π* electron transition of CN via distorted structure and nitrogen heterocycle	One-pot thermal-melting assemble following thermal-induce copolymerization of pyrazine-2,3-dicarboxylic acid and urea	300 W Xe lamp with 420 nm cutoff filter	97 % TC	100 min 50 mL	10 mg/L 10 mg	(Jiang et al., 2023)
Coral-like B-doped g-C_3N_4 with enhanced molecular dipole to boost photocatalysis-self-Fenton	Calcination of the precursor of boric acid, melamine and cyanuric acid	300 W Xe lamp with an AM1.5 filter	100 % 4-CP, mineralization rate 70.3 %, 2.6 and 4.9 times higher than that of Fenton process and photocatalysis	100 min 50 mL	20 mg/L 20 mg	(Jing et al., 2023)
Intramolecular D-A structure and n-π* transition co-promoted photodegradation activity of CN	One-pot thermal-induce copolymerization of urea and 2,5-thiophenedicarboxylic acid	300 W Xe lamp with 420 nm cutoff filter	92.1 % TC 77.5 % TOC	100 min 50 mL	10 mg/L 10 mg	(Shi et al., 2023)
Chlorine doped CN nanodisc	Calcination of melamine followed one step HCl treatment	–	98 % RhB, 2.18 folds	60 min	Catalyst ratio 300 mg/L	(Liu et al., 2022b)
Carbon-deficient and oxygen doped graphitic CN	Self-modification strategy of one-step formaldehyde-assisted thermal polycondensation of molten urea	300 W Xe lamp with both IR and 400 nm cutoff filters	p-nitrophenol (99.7 %) and atrazine (99.1)	– min 50 mL	10 mg/L 50 mg	(Wang et al., 2021a)
Self-assembly CN	Copolymerization of urea and 2-thiobarbitucid acid	300 W Xe lamp with 420 nm cutoff filter	SMZ 97 %	60 min 50 mL	10 mg/L 50 mg	(Zhou et al., 2019b)
Carbon and oxygen dual-doped CN	Copolymerization of urea precursor and ascorbic acid	300 W Xe lamp with 420 nm cutoff filter	BPA 100 %	60 min 50 mL	10 mg/L 50 mg	(Zhu et al., 2020)
Aromatic ring-terminated edges of CN nanosheets	One-step copolymerization process by employing quinazoline-2,4-diamine as a molecular-structure-blocking and aromatic ring terminated edge-directing agent	λ > 420 nm	TC 100 %, TOC removal 18 %	60 min	100 μM 0.5 g/L (Catalyst level)	(Chen et al., 2020c)
Salicylic acid modified CN	Copolymerizing urea and salicylic acid	300 W Xe lamp with 420 nm cutoff filter	Sulfamethazine 86 %	60 min –	100 μM 0.5 g/L (Catalyst level)	(Zhou et al., 2019a)

(*continued on next page*)

Table 2 (*continued*)

Designing strategy	Photocatalysts preparation	Condition	DegradationEfficiency, TOC removal rate	Catalysis timeVolume	Pollutant concentrationCatalyst dosage	Ref.
Porous intramolecular D-A CN via electron donors	Copolymerization of dicyandiamide with creatinine	Blue LED lamp (3 W*3, 26.3 mW/cm^2) at 450–480 nm	Sulfisoxazole 98.9 %, 5.6 times under blue light, 15.3 times under green light	80 min 50 mL	10 mg/L 20 mg	(Wang et al., 2022c)
Hierarchical CN microrods with carbon vacancies	Calcining melamine-NH_2OH·HCl precursor	300 W Xe lamp with 420 nm cutoff filter	87.9 % TC, 7.3 times	– min 200 mL	30 mg/L 50 mg	(Shen et al., 2021)
A dual strategy for synthesizing carbon/defect commodified CN porous nanotubes	Thermal-induce copolymerization of urea and succinic acid with a solvent-dispersion strategy	300 W Xe lamp with 420 nm cutoff filter	454 μmol h^{-1} g^{-1}, 84 folds	– min 80 mL	200 mg/L 20 mg	(Huo et al., 2021)

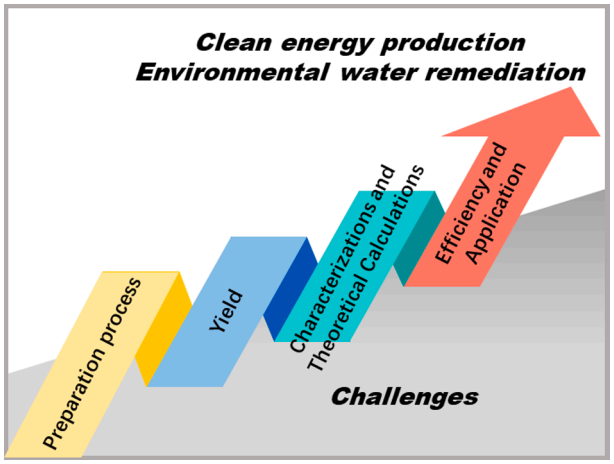

Fig. 9. Challenges of CN photocatalysts doped with small molecules.

efficiency of the system (Amirjani et al., 2023a, Amirjani and Sadrnezhaad, 2021, Amirjani et al., 2023b, Mirjalili et al., 2022). Moreover, a normative index and standard procedure to compare fairly the HER performance in different photocatalytic system will be built. Meanwhile, with the improvement of CN activity and the continuous development of its photoelectric performance, diverse CN-based devices have also been reported like sensors, solar cells, photodetectors, especially the large-scale and high-quality CN film is suitable for solid-state optoelectronic devices (Liu et al., 2024, Zhang et al., 2023b).

In the aspect of environmental water remediation, traditional photocatalytic degradation techniques are often non-selective in application, making it difficult for free radicals to identify target pollutants to be degraded. In the actual process of photodegradation and remediation of environmental water, high concentration substances (including beneficial components in the water body) tend to occupy the main catalytic active sites in most cases, consume most of the free radicals, and be degraded before target pollutants with low concentration and high toxicity. On the other hand, adsorption is extraordinarily important for photocatalytic processes because the adsorption rate for contaminants is one to several orders of magnitude lower than that of photogenerated electron-hole recombination rate. If the pollutants cannot migrate or adsorb to the surface of catalyst as quickly as possible, the photogenerated active substances cannot be fully utilized, which not only results in extremely low degradation efficiency, but also may generate incomplete degradation intermediates, causing secondary pollution. Recently, Professor Yang constructed a MIP-TiO_2@Fe_2O_3@g-C_3N_4 composite for photodegrading SMX in aqueous via loading Fe_2O_3 and g-C_3N_4 onto molecularly imprinted-TiO_2 (MT), and simultaneously address the problem of difficult absorption of visible light and easy recombination of carriers. Due to the crucial role of molecularly imprinted sites within the catalyst, the resultant MIP-TiO_2@Fe_2O_3@g-C_3N_4 composite can selectively capture and adsorption SMX, thus achieving a selective photodegradation rate of 96.8 %, nearly twice that of competing contaminants (Zhang et al., 2024). The development of CN photocatalytic materials with targeted recognition functionality would greatly beneficial for the targeted and deep removal of target pollutants from environmental water. With the continuous advancements in CN modification technology and diverse functional materials, the photocatalytic performance has reached unprecedented levels, enabling synergistic integration with photo-catalysis, Fenton, Fenton-like, adsorption, antibacterial, etc., for achieving highly effective remediation of environmental water.

The small molecule-doped CN, like most other CN photocatalyts, is an organic semiconductor photocatalytic material composed of earth-abundant and light elements. The advancement of "soft photocatalysis" in recent decades has showcased its superiority in terms of cost-effectiveness, reduced toxicity, and tunable electronic properties achieved through molecular engineering, while exhibits the same level of robustness, stability, and recoverability as its inorganic counterparts (Banerjee et al., 2020, Wang et al., 2019), aligning with the concept of sustainable development.

4. Conclusion

Green and sustainable photocatalytic technologies for clean energy production and environmental water remediation are effective ways to alleviate energy and environmental crises. CN, a non-metallic semiconductor photocatalyst, remains a prominent research focus in the fields of hydrogen production, hydrogen peroxide production, and pollutant degradation. This article provides an overview of recent advancements in improving the catalytic performance of CN by doping small molecules to form the CN skeleton (including benzene rings, heterocycles, and small molecule bonds, etc.), small molecules to provide doping elements (B, S, O, C, P, etc.) and introducing defects via doping small molecules in recent years. Through the continuous exploration of researchers, significant improvements have been achieved in the performance of CN materials doped with small molecules (Table 1 and Table 2). With increasing global attention towards energy conversion and environmental purification issues, it is anticipated that more researchers will dedicate their efforts to developing efficient CN-based photocatalytic materials for valuable contributions to sustainable development encompassing environment preservation, energy utilization efficiency enhancement, and human health improvement.

CRediT authorship contribution statement

Tianyu Zhou: Conceptualization, Data curation, Formal analysis, Project administration, Supervision, Writing – original draft, Writing –

review & editing. **Guangbo Che:** Conceptualization, Data curation, Funding acquisition, Supervision, Writing – review & editing. **Chunbo Liu:** Conceptualization, Formal analysis, Writing – original draft. **Lan Ding:** Visualization, Writing – original draft. **Honghui Teng:** Data curation.

Acknowledgements

This work is supported by the Natural Science Foundation Project of Jilin Province (20230101297JC, YDZJ202201ZYTS347, YDZJ202101-ZYTS073, 20210101117JC, YDZJ202201ZYTS349, YDZJ202102CX JD049), the National Natural Science Foundation (22004047), China Postdoctoral Science Foundation (2023M731299), the Project of Jilin Province Development and Reform Commission (2023C032-5, 2023C032-4, 2023C032-2), the Project of Human Resources and Social Security Department of Jilin Province (2023337, 20240601037RC), National College students' innovation and entrepreneurship training program (202310203008) and the Project of Education Department of Jilin Province (JJKH20220429KJ, JJKH20210460KJ).

References

Amirjani, A., Amlashi, N.B., Ahmadiani, Z.S., 2023a. Plasmon-enhanced photocatalysis based on plasmonic nanoparticles for energy and environmental solutions: a review. ACS Appl. Nano Mater. 6 (11), 9085–9123.

Amirjani, A., Sadrnezhaad, S.K., 2021. Computational electromagnetics in plasmonic nanostructures. J. Mater. Chem. C 9 (31), 9791–9819.

Amirjani, A., Shokrani, P., Sharif, S.A., Moheb, H., Ahmadi, H., Ahmadiani, Z.S., Paroushi, M.S., 2023b. Plasmon-enhanced nano-photosensitizers: game-changers in photodynamic therapy of cancers. J. Mater. Chem. B 11 (16), 3537–3566.

Bai, L., Huang, H., Yu, S., Zhang, D., Huang, H., Zhang, Y., 2022. Role of transition metal oxides in g-C_3N_4-based heterojunctions for photocatalysis and supercapacitors. J. Energy Chem. 64, 214–235.

Banerjee, T., Podjaski, F., Kröger, J., Biswal, B.P., Lotsch, B.V., 2020. Polymer photocatalysts for solar-to-chemical energy conversion. Nat. Rev. Mater. 6 (2), 168–190.

Bao, H., Wang, L., Li, G., Zhou, L., Xu, Y., Liu, Z., Wu, M., 2021. Carrier engineering of carbon nitride boosts visible-light photocatalytic hydrogen evolution. Carbon 179, 80–88.

Bhoyar, T., Kim, D.J., Abraham, B.M., Tonda, S., Manwar, N.R., Vidyasagar, D., Umare, S.S., 2022. Tailoring photoactivity of polymeric carbon nitride via donor-π-acceptor network. Appl. Catal. B-Environ. 310, 121347.

Che, H., Che, G., Zhou, P., Liu, C., Dong, H., Li, C., Song, N., Li, C., 2020. Nitrogen doped carbon ribbons modified g-C_3N_4 for markedly enhanced photocatalytic H_2 production in visible to near-infrared region. Chem. Eng. J. 382, 122870.

Che, H., Gao, X., Chen, J., Hou, J., Ao, Y., Wang, P., 2021a. Iodide-induced fragmentation of polymerized hydrophilic carbon nitride for high-performance quasi-homogeneous photocatalytic H_2O_2 production. Angew Chem Int. Ed. Engl. 60 (48), 25546–25550.

Che, H., Li, C., Li, C., Liu, C., Dong, H., Song, X., 2021b. Benzoyl isothiocyanate as a precursor to design of ultrathin and high-crystalline g-C_3N_4-based donor–acceptor conjugated copolymers for superior photocatalytic H_2 production. Chem. Eng. J. 410, 127791.

Che, L., Pan, J., Cai, K., Cong, Y., Lv, S.-W., 2023b. The construction of p-n heterojunction for enhancing photocatalytic performance in environmental application: a review. Sep. Purif. Technol. 315, 123708.

Che, H., Wang, P., Chen, J., Gao, X., Liu, B., Ao, Y., 2022. Rational design of donor-acceptor conjugated polymers with high performance on peroxydisulfate activation for pollutants degradation. Appl. Catal. B-Environ. 316, 121611.

Che, H., Wang, J., Wang, P., Ao, Y., Chen, J., Gao, X., Zhu, F., Liu, B., 2023a. Simultaneously achieving fast intramolecular charge transfer and mass transport in holey D-pi-A organic conjugated polymers for highly efficient photocatalytic pollutant degradation. JACS Au 3 (5), 1424–1434.

Chen, Z., Fan, T.T., Yu, X., Wu, Q.L., Zhu, Q.H., Zhang, L.Z., Li, J.H., Fang, W.-P., Yi, X. D., 2018. Gradual carbon doping of graphitic carbon nitride towards metal-free visible light photocatalytic hydrogen evolution. J. Mater. Chem. A 6 (31), 15310–15319.

Chen, Y., He, X., Guo, D., Cai, Y., Chen, J., Zheng, Y., Gao, B., Lin, B., 2020a. Supramolecular electrostatic self-assembly of mesoporous thin-walled graphitic carbon nitride microtubes for highly efficient visible-light photocatalytic activities. J. Energy Chem. 49, 214–223.

Chen, Z., Li, S., Peng, Y., Hu, C., 2020c. Tailoring aromatic ring-terminated edges of g-C_3N_4 nanosheets for efficient photocatalytic hydrogen evolution with simultaneous antibiotic removal. Catal. Sci. Tech. 10 (16), 5470–5479.

Chen, Z., Luo, Y., Huang, C., Shen, X., 2021b. In situ assembly of ZnO/graphene oxide on synthetic molecular receptors: Towards selective photoreduction of Cr(VI) via interfacial synergistic catalysis. Chem. Eng. J. 414, 128914.

Chen, Y., Qu, Y., Zhou, X., Li, D., Xu, P., Sun, J., 2020b. Phenyl-bridged graphitic carbon nitride with a porous and hollow sphere structure to enhance dissociation of photogenerated charge carriers and visible-light-driven H_2 generation. ACS Appl. Mater. Inter. 12 (37), 41527–41537.

Chen, Y., Qu, Y., Xu, P., Zhou, X., Sun, J., 2021a. Insight into the influence of donor-acceptor system on graphitic carbon nitride nanosheets for transport of photoinduced charge carriers and photocatalytic H_2 generation. J. Colloid Interface Sci. 601, 326–337.

Chen, L., Ren, J.T., Yuan, Z.Y., 2023. Enabling internal electric fields to enhance energy and environmental catalysis. Adv. Energy Mater. 13 (11), 03720.

Chen, J., Tao, X., Tao, L., Li, H., Li, C., Wang, X., Li, C., Li, R., Yang, Q., 2019. Novel conjugated organic polymers as candidates for visible-light-driven photocatalytic hydrogen production. Appl. Catal. B-Environ. 241, 461–470.

Chen, J., Kang, N., Fan, J., Lu, C., Lv, K., 2022. Carbon nitride for photocatalytic water splitting to produce hydrogen and hydrogen peroxide. Mater. Today Chem. 26, 101028.

Cheng, C., Shi, J., Wen, L., Dong, C.L., Huang, Y.C., Zhang, Y., Zong, S., Diao, Z., Shen, S., Guo, L., 2021. Disordered nitrogen-defect-rich porous carbon nitride photocatalyst for highly efficient H_2 evolution under visible-light irradiation. Carbon 181, 193–203.

Deng, Y., Tang, L., Zeng, G., Zhu, Z., Yan, M., Zhou, Y., Wang, J., Liu, Y., Wang, J., 2017. Insight into highly efficient simultaneous photocatalytic removal of Cr(VI) and 2,4-diclorophenol under visible light irradiation by phosphorus doped porous ultrathin g-C3N4 nanosheets from aqueous media: Performance and reaction mechanism. Appl. Catal. B-Environ. 203, 343–354.

Di, J., Xia, J., Li, X., Ji, M., Xu, H., Chen, Z., Li, H., 2016. Constructing confined surface carbon defects in ultrathin graphitic carbon nitride for photocatalytic free radical manipulation. Carbon 107, 1–10.

Dong, G., Qiu, P., Chen, Q., Huang, C., Chen, F., Liu, X., Li, Z., Wang, Y., Zhao, Y., 2022a. K+-Intercalated carbon nitride with electron storage property for high-efficiency visible light driven nitrogen fixation. Chem. Eng. J. 433, 133573.

Dong, P., Zhang, A., Cheng, T., Pan, J., Song, J., Zhang, L., Guan, R., Xi, X., Zhang, J., 2022b. 2D/2D S-scheme heterojunction with a covalent organic framework and g-C_3N_4 nanosheets for highly efficient photocatalytic H_2 evolution. Chin. J. Catal. 43 (10), 2592–2605.

Dong, H., Zuo, Y., Song, N., Hong, S., Xiao, M., Zhu, D., Sun, J., Chen, G., Li, C., 2021a. Bimetallic synergetic regulating effect on electronic structure in cobalt/vanadium co-doped carbon nitride for boosting photocatalytic performance. Appl. Catal. B-Environ. 287, 119954.

Dong, H., Zuo, Y., Xiao, M., Zhou, T., Cheng, S., Chen, G., Sun, J., Yan, M., Li, C., 2021b. Limbic inducted and delocalized effects of diazole in carbon nitride skeleton for propelling photocatalytic hydrogen evolution. ACS Appl. Mater. Interf. 13 (47), 56273–56284.

Du, J., Li, S., Du, Z., Meng, S., Li, B., 2021. Boron/oxygen-codoped graphitic carbon nitride nanomesh for efficient photocatalytic hydrogen evolution. Chem. Eng. J. 407, 127114.

Fakhrabadi, M.M.S., Allahverdizadeh, A., Kamkari, B., Vahabi, M., 2013. Investigation of mechanical properties and thermal conductivities of nitrogen doped carbon nanotubes. J. Comput. Theor. Nanosci. 10 (11), 2536–2541.

Fang, H.-B., Zhang, X.-H., Wu, J., Li, N., Zheng, Y.-Z., Tao, X., 2018. Fragmented phosphorus-doped graphitic carbon nitride nanoflakes with broad sub-bandgap absorption for highly efficient visible-light photocatalytic hydrogen evolution. Appl. Catal. B-Environ. 225, 397–405.

Fei, T., Qin, C., Zhang, Y., Dong, G., Wang, Y., Zhou, Y., Cui, M., 2021. A 3D peony-like sulfur-doped carbon nitride synthesized by self-assembly for efficient photocatalytic hydrogen production. Int. J. Hydrogen Energ. 46 (39), 20481–20491.

Fu, J., Zhu, B., Jiang, C., Cheng, B., You, W., Yu, J., 2017. Hierarchical porous O-doped g-C_3N_4 with enhanced photocatalytic CO_2 reduction activity. Small 13 (15).

Ge, F., Huang, S., Yan, J., Jing, L., Chen, F., Xie, M., Xu, Y., Xu, H., Li, H., 2021. Sulfur promoted n-π* electron transitions in thiophene-doped g-C3N4 for enhanced photocatalytic activity. Chinese J. Catal. 42 (3), 450–459.

Ghaderi, H., Ghasemi, A., Rouhi, S., Mahdavi, E., 2021. Evaluation of the thermal conductivity coefficient of the strained concentric multi-walled carbon and boron-nitride nanotubes: a molecular dynamics investigation. Physica E Low Dimens. Syst. Nanostruct. 134, 114830.

Guan, G., Pan, J.H., Li, Z., 2021. Innovative utilization of molecular imprinting technology for selective adsorption and (photo)catalytic eradication of organic pollutants. Chemosphere 265, 129077.

Guo, Q., Wei, M., Zheng, Z., Huang, X., Song, X., Qiu, S.B., Yang, X.b., Liu, X., Qiu, J. and Dong, G. (2019) Full-color chemically modulated g-C_3N_4 for white-light-emitting device. Adv. Optical Mater. 7(21).

Guo, L., Niu, Y., Xu, H., Li, Q., Razzaque, S., Huang, Q., Jin, S., Tan, B., 2018. Engineering heteroatoms with atomic precision in donor–acceptor covalent triazine frameworks to boost photocatalytic hydrogen production. J. Mater. Chem. A 6 (40), 19775–19781.

Hu, C., Wang, X., Song, B., 2020. High-performance position-sensitive detector based on the lateral photoelectrical effect of two-dimensional materials. Light Sci Appl 9, 88.

Huang, S., Ge, F., Yan, J., Li, H., Zhu, X., Xu, Y., Xu, H., Li, H., 2021. Synthesis of carbon nitride in moist environments: A defect engineering strategy toward superior photocatalytic hydrogen evolution reaction. J. Energy Chem. 54, 403–413.

Huo, T., Ba, G., Deng, Q., Yu, F., Wang, G., Li, H., Hou, W., 2021. A dual strategy for synthesizing carbon/defect comodified polymeric carbon nitride porous nanotubes with boosted photocatalytic hydrogen evolution and synchronous contaminant degradation. Appl. Catal. B-Environ. 287, 119995.

Ismael, M., 2020a. The photocatalytic performance of the ZnO/g-C_3N_4 composite photocatalyst toward degradation of organic pollutants and its inactivity toward hydrogen evolution: The influence of light irradiation and charge transfer. Chem. Phys. Lett. 739, 136992.

Ismael, M., 2020b. A review on graphitic carbon nitride (g-C3N4) based nanocomposites: Synthesis, categories, and their application in photocatalysis. J. Alloys Compd. 846, 156446.
Ismael, M., 2021. Ferrites as solar photocatalytic materials and their activities in solar energy conversion and environmental protection: A review. Sol. Energy Mater. Sol. Cells 219, 110786.
Ismael, M., 2022a. Photo-Fenton reaction enhanced visible-light activity of p- Photo-Fenton reaction enhanced visible-light activity of p-$CuFe_2O_4$/n-g-C_3N_4 heterojunction composites synthesized by a simple ultrasonic-assisted route for organic pollutants degradation. Mater. Res. Bull. 151, 111803.
Ismael, M., 2022b. Structure, properties, and characterization of mullite-type materials $Bi_2M_4O_9$ and their applications in photocatalysis: A review. J. Environ. Chem. Eng. 10 (6), 108640.
Ismael, M., 2023a. Environmental remediation and sustainable energy generation via photocatalytic technology using rare earth metals modified g-C_3N_4: A review. J. Alloys Compd. 931, 167469.
Ismael, M., 2023b. Facile synthesis of NiO-loaded g-C_3N_4 heterojunction photocatalyst for efficient photocatalytic degradation of 4-nitrophenol under visible light irradiation. J Photochem. Photobiol. A 439, 114576.
Ismael, M., Wark, M., 2022. Photocatalytic activity of $CoFe_2O_4$/g-C_3N_4 nanocomposite toward degradation of different organic pollutants and their inactivity toward hydrogen production: The role of the conduction band position. FlatChem 32, 100337.
Ismael, M., Wu, Y., 2019. A facile synthesis method for fabrication of $LaFeO_3$/g-C_3N_4nanocomposite as efficient visible-light-driven photocatalyst for photodegradation of RhB and 4-CP. New J. Chem. 43 (35), 13783–13793.
Ismael, M., Wu, Y., Wark, M., 2019. Photocatalytic activity of ZrO_2 composites with graphitic carbon nitride for hydrogen production under visible light. New J. Chem. 43 (11), 4455–4462.
Jatoi, A.S., Mubarak, N.M., Hashmi, Z., Solangi, N.H., Karri, R.R., Tan, Y.H., Mazari, S.A., Koduru, J.R., Alfantazi, A., 2023. New insights into MXene applications for sustainable environmental remediation. Chemosphere 313, 137497.
Jia, G., Wang, Y., Cui, X., Yang, Z., Liu, L., Zhang, H., Wu, Q., Zheng, L., Zheng, W., 2019. Asymmetric embedded benzene ring enhances charge transfer of carbon nitride for photocatalytic hydrogen generation. Appl. Catal. B-Environ. 258, 117959.
Jiang, R., Lu, G., Liu, J., Wu, D., Yan, Z., Wang, Y., 2021a. Incorporation of π-conjugated molecules as electron donors in g-C_3N_4 enhances photocatalytic H_2-production. Renewable Energy 164, 531–540.
Jiang, L., Yuan, X., Pan, Y., Liang, J., Zeng, G., Wu, Z., Wang, H., 2017. Doping of graphitic carbon nitride for photocatalysis: A review. Appl. Catal. B-Environ. 217, 388–406.
Jiang, W., Zhao, Y., Zong, X., Nie, H., Niu, L., An, L., Qu, D., Wang, X., Kang, Z., Sun, Z., 2021b. Photocatalyst for high-performance H_2 production: Ga-doped polymeric carbon nitride. Angew. Chem., Int. Ed. 60 (11), 6124–6129.
Jiang, J., Zhou, S., Chen, Z., Gu, P., Li, Y., Xu, Q., 2023. Facile fabrication of a visible-light stable metal-free g-C_3N_4/COF heterojunction with efficiently enhanced photocatalytic activity. New J. Chem. 47 (16), 7538–7547.
Jin, T., Liu, C., Chen, F., Qian, J., Qiu, Y., Meng, X., Chen, Z., 2022. Synthesis of g-C_3N_4/CQDs composite and its photocatalytic degradation property for Rhodamine B. Carbon Letters 32 (6), 1451–1462.
Jing, M., Zhao, H., Jian, L., Pan, C., Dong, Y., Zhu, Y., 2023. Coral-like B-doped g-C_3N_4 with enhanced molecular dipole to boost photocatalysis-self-Fenton removal of persistent organic pollutants. J Hazard Mater. 449, 131017.
Khani, N., Seyyed Fakhrabadi, M.M., Vahabi, M., Kamkari, B., 2014. Modal analysis of silicon carbide nanotubes using structural mechanics. Appl. Phys. A 116 (4), 1687–1694.
Khayoon, H.A., Ismael, M., Al-nayili, A., Alshamsi, H.A., 2023. Fabrication of $LaFeO_3$-nitrogen deficient g-C_3N_4 composite for enhanced the photocatalytic degradation of RhB under sunlight irradiation. Inorg. Chem. Commun. 157, 111356.
Kim, H., Gim, S., Jeon, T.H., Kim, H., Choi, W., 2017. Distorted carbon nitride structure with substituted benzene moieties for enhanced visible light photocatalytic activities. ACS Appl. Mater. Inter. 9 (46), 40360–40368.
Kumar, A., Raizada, P., Hosseini-Bandegharaei, A., Thakur, V.K., Nguyen, V.-H., Singh, P., 2021. C-, N-Vacancy defect engineered polymeric carbon nitride towards photocatalysis: viewpoints and challenges. J. Mater. Chem. A 9 (1), 111–153.
Kuspanov, Z., Bakbolat, B., Baimenov, A., Issadykov, A., Yeleuov, M., Daulbayev, C., 2023. Photocatalysts for a sustainable future: Innovations in large-scale environmental and energy applications. Sci Total Environ. 885, 163914.
Lei, Q., Yang, S., Ding, D., Tan, J., Liu, J., Chen, R., 2021. Local-interaction-field-coupled semiconductor photocatalysis: recent progress and future challenges. J. Mater. Chem. A 9 (5), 2491–2525.
Li, F., Han, M., Jin, Y., Zhang, L., Li, T., Gao, Y., Hu, C., 2019. Internal electric field construction on dual oxygen group-doped carbon nitride for enhanced photodegradation of pollutants under visible light irradiation. Appl. Catal. B-Environ. 256, 117705.
Li, J., Shen, B., Hong, Z., Lin, B., Gao, B., Chen, Y., 2012. A facile approach to synthesize novel oxygen-doped g-C_3N_4 with superior visible-light photoreactivity. Chem. Commun. 48 (98), 12017–12019.
Li, K., Sun, M., Zhang, W.-D., 2018. Polycyclic aromatic compounds-modified graphitic carbon nitride for efficient visible-light-driven hydrogen evolution. Carbon 134, 134–144.
Li, C., Wu, H., Zhu, D., Zhou, T., Yan, M., Chen, G., Sun, J., Dai, G., Ge, F., Dong, H., 2021a. High-efficient charge separation driven directionally by pyridine rings grafted on carbon nitride edge for boosting photocatalytic hydrogen evolution. Appl. Catal. B-Environ. 297, 120433.
Li, K., Zhang, W.D., 2018. Creating graphitic carbon nitride based donor-π-acceptor-π-donor structured catalysts for highly photocatalytic hydrogen evolution. Small 14 (12), 1703599.
Li, Q., Zhang, L., Liu, J., Zhou, J., Jiao, Y., Xiao, X., Zhao, C., Zhou, Y., Ye, S., Jiang, B., Liu, J., 2021b. Porous carbon nitride thin strip: precise carbon doping regulating delocalized pi-electron induces elevated photocatalytic hydrogen evolution. Small 17 (11), e2006622.
Li, M., Zheng, Q., Durkin, D.P., Chen, H., Shuai, D., 2022c. Environmental application of chlorine-doped graphitic carbon nitride: Continuous solar-driven photocatalytic production of hydrogen peroxide. J Hazard Mater. 436, 129251.
Li, C., Zhou, T., Yan, M., Cheng, S., Wang, Y., Sun, J., Chen, G., Dong, H., 2022a. Intramolecular π-conjugated channel expansion achieved by doping cross-linked dopants into carbon nitride frameworks for propelling photocatalytic hydrogen evolution and mechanism insight. Inorg. Chem. Front. 9 (1), 60–69.
Li, C., Zhu, D., Cheng, S., Zuo, Y., Wang, Y., Ma, C., Dong, H., 2022b. Recent research progress of bimetallic phosphides-based nanomaterials as cocatalyst for photocatalytic hydrogen evolution. Chin. Chem. Lett. 33 (3), 1141–1153.
Liang, Z., Zhuang, X., Tang, Z., Li, H., Liu, L., Kang, W., 2021. Soft-template induced synthesis of high-crystalline polymeric carbon nitride with boosted photocatalytic performance. J. Mater. Chem. A 9 (11), 6805–6810.
Lin, X., Hou, X., Cui, L., Zhao, S., Bi, H., Du, H., Yuan, Y., 2021a. Increasing π-electron availability in benzene ring incorporated graphitic carbon nitride for increased photocatalytic hydrogen generation. J. Mater. Sci. Technol. 65, 164–170.
Lin, J., Tian, W., Guan, Z., Zhang, H., Duan, X., Wang, H., Sun, H., Fang, Y., Huang, Y., Wang, S., 2022. Functional carbon nitride materials in Photo-Fenton-Like catalysis for environmental remediation. Adv. Funct. Mater. 32 (24), 2201743.
Lin, Y., Yang, Y., Guo, W., Wang, L., Zhang, R., Liu, Y., Zhai, Y., 2021b. Preparation of double-vacancy modified carbon nitride to greatly improve the activity of photocatalytic hydrogen generation. Appl. Surf. Sci. 560, 150029.
Liu, D., Li, C., Zhu, L., Sun, R., Wang, H., Xie, L., Ge, S., Yu, J., 2024. Graphitic carbon nitride photoelectric properties regulation for highly sensitive sensing applications. Microchem. J. 199, 110088.
Liu, X., Ma, R., Zhuang, L., Hu, B., Chen, J., Liu, X., Wang, X., 2020. Recent developments of doped g-C_3N_4 photocatalysts for the degradation of organic pollutants. Crit. Rev. Environ. Sci. Technol. 51 (8), 751–790.
Liu, W., Peng, R., Ye, X., Guo, J., Luo, L., 2021. Sulfur doping and structure defect functionalized carbon nitride nanosheets with enhanced photocatalytic degradation activity. Appl. Surf. Sci. 560, 150013.
Liu, W., Wang, P., Chen, J., Gao, X., Che, H., Liu, B., Ao, Y., 2022a. Unraveling the mechanism on ultrahigh efficiency photocatalytic H_2O_2 generation for dual-heteroatom incorporated polymeric carbon nitride. Adv. Funct. Mater. 32 (38), 2205119.
Liu, W., Wen, F., Wang, J., 2022b. Construction of chlorine doped graphitic carbon nitride nanodisc for enhanced photocatalytic activity and mechanism insight. Int. J. Hydrogen Energy 47 (38), 16887–16899.
Liu, C., Zhang, Y., Dong, F., Reshak, A.H., Ye, L., Pinna, N., Zeng, C., Zhang, T., Huang, H., 2017. Chlorine intercalation in graphitic carbon nitride for efficient photocatalysis. Appl. Catal. B-Environ. 203, 465–474.
Liu, Z., Zhang, J., Wan, Y., Chen, J., Zhou, Y., Zhang, J., Wang, G., Wang, R., 2022c. Donor-Acceptor structural polymeric carbon nitride with in-plane electric field accelerating charge separation for efficient photocatalytic hydrogen evolution. Chem. Eng. J. 430, 132725.
Lu, Z., He, F., Hsieh, C.Y., Wu, X., Song, M., Liu, X., Liu, Y., Yuan, S., Dong, H., Han, S., Du, P., Xing, G., 2019. Magnetic hierarchical photocatalytic nanoreactors: Toward highly selective Cd2+ removal with secondary pollution free tetracycline degradation. ACS App. Nano Mater. 2 (3), 1664–1674.
Lu, Z., Zhou, G., Li, B., Xu, Y., Wang, P., Yan, H., Song, M., Ma, C., Han, S., Liu, X., 2022. Heterotopic reaction strategy for enhancing selective reduction and synergistic oxidation ability through trapping Cr (VI) into specific reaction site: A stable and self-cleaning ion imprinted CdS/HTNW photocatalytic membrane. Appl. Catal. B-Environ. 301, 120787.
Luo, L., Wang, K., Gong, Z., Zhu, H., Ma, J., Xiong, L., Tang, J., 2021. Bridging-nitrogen defects modified graphitic carbon nitride nanosheet for boosted photocatalytic hydrogen production. Int. J. Hydrogen Energ. 46 (53), 27014–27025.
Ma, Y., Liu, F., Liu, Y., Lan, X., Zhu, Y., Shi, J., Jiang, W., Wang, G., Park, S.H., 2021. In-situ intramolecular synthesis of tubular carbon nitride S-scheme homojunctions with exceptional in-plane exciton splitting and mechanism insight. Chem. Eng. J. 414, 128802.
Ma, D., Zhang, Z., Zou, Y., Chen, J., Shi, J., 2024. The progress of g-C_3N_4 in photocatalytic H_2 evolution: From fabrication to modification. Coord. Chem. Rev. 500, 215489.
Ma, Z., Zong, X., Hong, Q., Niu, L., Yang, T., Jiang, W., Qu, D., An, L., Wang, X., Kang, Z., Sun, Z., 2022. Electrostatic potential of the incorporated asymmetry molecules induced high charge separation efficiency of the modified carbon nitride copolymers. Appl. Catal. B-Environ. 319, 121922.
Mahvelati-Shamsabadi, T., Lee, B.-K., 2020. Photocatalytic H_2 evolution and CO_2 reduction over phosphorus-doped g-C_3N_4 nanostructures: Electronic, Optical, and Surface properties. Renew. Sust. Energ. Rev. 130, 109957.
Mirjalili, S., Tohidi Moghadam, T. and H. Sajedi, R. (2022) Facile and rapid detection of microalbuminuria by antibody-functionalized gold nanorods. plasmonics 17(3), 1269-1277.
Nagella, S.R., Vijitha, R., Ramesh Naidu, B., Krishna Rao, K.S.V., Ha, C.-S., Venkateswarlu, K., 2023. Benchmarking recent advances in hydrogen production using g-C_3N_4-based photocatalysts. Nano Energy 111, 108402.
Ni, T., Zhang, H., Yang, Z., Zhou, L., Pan, L., Li, C., Yang, Z., Liu, D., 2022. Enhanced adsorption and catalytic degradation of antibiotics by porous 0D/3D Co_3O_4/g-C_3N_4

activated peroxymonosulfate: An experimental and mechanistic study. J Colloid Interface Sci. 625, 466–478.
Noureen, L., Wang, Q., Humayun, M., Shah, W.A., Xu, Q., Wang, X., 2023. Recent advances in structural engineering of photocatalysts for environmental remediation. Environ Res. 219, 115084.
Ouedraogo, S., Chouchene, B., Desmarets, C., Gries, T., Balan, L., Fournet, R., Medjahdi, G., Bayo, K., Schneider, R., 2018. Copper octacarboxyphthalocyanine as sensitizer of graphitic carbon nitride for efficient dye degradation under visible light irradiation. Appl. Catal. A-Gen. 563, 127–136.
Palani, G., Apsari, R., Hanafiah, M.M., Venkateswarlu, K., Lakkaboyana, S.K., Kannan, K., Shivanna, A.T., Idris, A.M., Yadav, C.H., 2022. Metal-doped graphitic carbon nitride nanomaterials for photocatalytic environmental applications – a review. Nanomaterials 12 (10), 17544.
Patnaik, S., Sahoo, D.P., Parida, K., 2021. Recent advances in anion doped g-C_3N_4 photocatalysts: a review. Carbon 172, 682–711.
Peng, X., Li, J., Liu, X., Yi, L., Cai, P., Wen, Z., 2021. Cl-doped carbon nitride nanostrips for remarkably improving visible-light photocatalytic hydrogen production. Int. J. Hydrogen Energ. 46 (56), 28591–28601.
Peng, J., Lu, Z., Lu, J., Ma, Z., Song, M., Liu, X., Huo, P., Dong, H., Qiu, X., Han, S., 2019. Enhanced selectivity for photodegrading ciprofloxacin by a magnetic photocatalyst modified with a POPD–CdS heterojunction embedded imprinted layer. New J. Chem. 43 (6), 2610–2623.
Peng, J., Deng, F., Shi, H., Wang, Z., Li, X., Zou, J., Luo, X., 2024. Target recognition and preferential degradation of toxic chemical groups by innovative group-imprinted photocatalyst with footprint cavity. Appl. Catal. B-Environ. 340, 123179.
Praus, P., 2022. A brief review of s-triazine graphitic carbon nitride. Carbon Letters 32 (3), 703–712.
Qi, K., Cui, N., Zhang, M., Ma, Y., Wang, G., Zhao, Z., Khataee, A., 2021. Ionic liquid-assisted synthesis of porous boron-doped graphitic carbon nitride for photocatalytic hydrogen production. Chemosphere 272, 129953.
Qin, J., Wang, S., Ren, H., Hou, Y., Wang, X., 2015. Photocatalytic reduction of CO_2 by graphitic carbon nitride polymers derived from urea and barbituric acid. Appl. Catal. B-Environ. 179, 1–8.
Ramin Babazadeh, D., Nastaran, S., 2023a. Laboratory preparation of LSM and LSF sputtering targets using PTFE rings for deposition of SOFC thin film electrodes. World J. Adv. Eng. Technol. Sci. 10 (2), 203–212.
Ramin Babazadeh, D., Nastaran, S., 2023b. Optimizing LSM-LSF composite cathodes for enhanced solid oxide fuel cell performance: Material engineering and electrochemical insights. World J. Adv. Res. Rev. 20 (1), 1284–1291.
Rana, A., Sudhaik, A., Raizada, P., Nguyen, V.H., Xia, C., Parwaz Khan, A.A., Thakur, S., Nguyen-Tri, P., Nguyen, C.C., Kim, S.Y., Le, Q.V., Singh, P., 2022. Graphitic carbon nitride based immobilized and non-immobilized floating photocatalysts for environmental remediation. Chemosphere 297, 134229.
Ruan, X., Cui, X., Jia, G., Wu, J., Zhao, J., Singh, D.J., Liu, Y., Zhang, H., Zhang, L., Zheng, W., 2022. Intramolecular heterostructured carbon nitride with heptazine-triazine for enhanced photocatalytic hydrogen evolution. Chem. Eng. J. 428, 132579.
Shen, Q., Li, N., Bibi, R., Richard, N., Liu, M., Zhou, J., Jing, D., 2020. Incorporating nitrogen defects into novel few-layer carbon nitride nanosheets for enhanced photocatalytic H_2 production. Appl. Surf. Sci. 529, 147104.
Shen, Q., Wei, L., Bibi, R., Wang, K., Hao, D., Zhou, J., Li, N., 2021. Boosting photocatalytic degradation of tetracycline under visible light over hierarchical carbon nitride microrods with carbon vacancies. J. Hazard Mater. 413, 125376.
Shi, J., Tai, M., Hou, J., Qiao, Y., Liu, C., Zhou, T., Wang, L., Hu, B., 2023. Intramolecular D-A structure and n-π* transition co-promoted photodegradation activity of carbon nitride: Performance, mechanism and toxicity insight. Chem. Eng. J. 456, 141029.
Song, P., Liang, S., Cui, J., Ren, D., Duan, R., Yang, Q., Sun, S., 2019. Purposefully designing novel hydroxylated and carbonylated melamine towards the synthesis of targeted porous oxygen-doped g-C_3N_4 nanosheets for highly enhanced photocatalytic hydrogen production. Catal. Sci. Technol. 9 (18), 5150–5159.
Song, P., Sun, S., Cui, J., Zheng, X., Liang, S., 2021. Organic dye-reformed construction of porous-defect g-C_3N_4 nanosheet for improved visible-light-driven photocatalytic activity. Appl. Surf. Sci. 568, 150986.
Sun, S., Li, J., Cui, J., Gou, X., Yang, Q., Liang, S., Yang, Z., Zhang, J., 2018b. Constructing oxygen-doped g-C_3N_4 nanosheets with an enlarged conductive band edge for enhanced visible-light-driven hydrogen evolution. Inorg. Chem. Front. 5 (7), 1721–1727.
Sun, S., Gou, X., Tao, S., Cui, J., Li, J., Yang, Q., Liang, S., Yang, Z., 2019a. Mesoporous graphitic carbon nitride (g-C3N4) nanosheets synthesized from carbonated beverage-reformed commercial melamine for enhanced photocatalytic hydrogen evolution. Mater. Chem. Front. 3 (4), 597–605.
Sun, Z., Jiang, Y., Zeng, L., Huang, L., 2019b. Intramolecular charge transfer and extended conjugate effects in donor-pi-acceptor-type mesoporous carbon nitride for photocatalytic hydrogen evolution. ChemSusChem 12 (7), 1325–1333.
Sun, Z., Jiang, Y., Zeng, L., Huang, L., 2019c. Intramolecular charge transfer and extended conjugate effects in donor-π-acceptor-type mesoporous carbon nitride for photocatalytic hydrogen evolution. ChemSusChem 12 (7), 1325–1333.
Sun, S., Liang, S., 2017. Recent advances in functional mesoporous graphitic carbon nitride (mpg-C3N4) polymers. Nanoscale 9 (30), 10544–10578.
Sun, Z., Tan, Y., Wan, J., Huang, L., 2021. In-depth understanding of the effects of intramolecular charge transfer on carbon nitride based Photocatalysts. Chinese J. Chem. 39 (7), 2044–2053.
Sun, C., Zhang, H., Liu, H., Zheng, X., Zou, W., Dong, L., Qi, L., 2018a. Enhanced activity of visible-light photocatalytic H_2 evolution of sulfur-doped photocatalyst g-C_3N_4 via nanoparticle metal Ni as cocatalyst. Appl. Catal. B-Environ. 235, 66–74.
Teng, Z., Yang, N., Lv, H., Wang, S., Hu, M., Wang, C., Wang, D., Wang, G., 2019. Edge-functionalized g-C_3N_4 nanosheets as a highly efficient metal-free photocatalyst for safe drinking water. Chem. 5 (3), 664–680.
Tong, C., Jing, L., Xie, M., He, M., Liu, Y., Yuan, J., Song, Y., Xu, Y., 2022. C-O band structure modified broad spectral response carbon nitride with enhanced electron density in photocatalytic peroxymonosulfate activation for bisphenol pollutants removal. J. Hazard Mater. 432, 128663.
Wan, S., Xu, J., Cao, S., Yu, J., 2022. Promoting intramolecular charge transfer of graphitic carbon nitride by donor–acceptor modulation for visible-light photocatalytic H2 evolution. Interdiscip. Mater. 1 (2), 294–308.
Wang, X., Chen, L., Chong, S.Y., Little, M.A., Wu, Y., Zhu, W.-H., Clowes, R., Yan, Y., Zwijnenburg, M.A., Sprick, R.S., Cooper, A.I., 2018. Sulfone-containing covalent organic frameworks for photocatalytic hydrogen evolution from water. Nat. Chem. 10 (12), 1180–1189.
Wang, X., Meng, J., Zhang, X., Liu, Y., Ren, M., Yang, Y., Guo, Y., 2021a. Controllable approach to carbon-deficient and oxygen-doped graphitic carbon nitride: Robust photocatalyst against recalcitrant organic pollutants and the mechanism insight. Adv. Funct. Mater. 31 (20), 10763.
Wang, H., Thangamuthu, M., Wu, Z., Yang, J., Yuan, H., Bayazit, M.K., Tang, J., 2022a. Self-assembled sulphur doped carbon nitride for photocatalytic water reforming of methanol. Chem. Eng. J. 445, 136790.
Wang, Y., Wang, H., Chen, F., Cao, F., Zhao, X., Meng, S., Cui, Y., 2017. Facile synthesis of oxygen doped carbon nitride hollow microsphere for photocatalysis. Appl. Catal. B-Environ. 206, 417–425.
Wang, Y., Vogel, A., Sachs, M., Sprick, R.S., Wilbraham, L., Moniz, S.J.A., Godin, R., Zwijnenburg, M.A., Durrant, J.R., Cooper, A.I., Tang, J., 2019. Current understanding and challenges of solar-driven hydrogen generation using polymeric photocatalysts. Nat. Energy 4 (9), 746–760.
Wang, X.L., Yang, H.G., 2017. Facile fabrication of high-yield graphitic carbon nitride with a large surface area using bifunctional urea for enhanced photocatalytic performance. Appl. Catal. B-Environ. 205, 624–630.
Wang, J., Yu, Y., Cui, J., Li, X., Zhang, Y., Wang, C., Yu, X., Ye, J., 2022b. Defective g-C_3N_4/covalent organic framework van der Waals heterojunction toward highly efficient S-scheme CO_2 photoreduction. Appl. Catal. B-Environ. 301, 120814.
Wang, X., Zhao, Y., Tan, H., Sun, H., Shang, Q., Zhao, X., Qiu, T., Li, Y., 2021b. Foamer-derived bulk nitrogen defects and oxygen-doped porous carbon nitride with greatly extended visible-light response and efficient photocatalytic activity. ACS Appl. Mater. Inter. 13 (20), 23866–23876.
Wang, Z., Zheng, X., Chen, P., Li, D., Zhang, Q., Liu, H., Zhong, J., Lv, W., Liu, G., 2022c. Synchronous construction of a porous intramolecular D-A conjugated polymer via electron donors for superior photocatalytic decontamination. J. Hazard Mater. 424 (Pt B), 127379.
Wang, Y., Zhou, T., Wang, H., Wang, L., Qi, J., Cui, K., Liu, C., Hu, B., 2023. Fabricating fragmented intramolecular D-A integrated carbon nitride photocatalysts with elevating activity: performance and mechanism analysis. Int. J. Hydrogen Energ. 51, 61–71.
Wu, L., An, S., Song, Y., 2021b. Heteropolyacids-immobilized graphitic carbon nitride: highly efficient photo-oxidation of benzyl alcohol in the aqueous phase. Engineering 7 (1), 94–102.
Wu, Y., Chen, J., Che, H., Gao, X., Ao, Y., Wang, P., 2022. Boosting 2e$^-$ oxygen reduction reaction in garland carbon nitride with carbon defects for high-efficient photocatalysis-self-Fenton degradation of 2,4-dichlorophenol. Appl. Catal. B-Environ. 307, 121185.
Wu, B., Zhang, L., Jiang, B., Li, Q., Tian, C., Xie, Y., Li, W., Fu, H., 2021a. Ultrathin porous carbon nitride bundles with an adjustable energy band structure toward simultaneous solar photocatalytic water splitting and selective phenylcarbinol oxidation. Angew. Chem. Int. Edit. 60 (9), 4815–4822.
Xing, Y., Wang, X., Hao, S., Zhang, X., Wang, X., Ma, W., Zhao, G., Xu, X., 2021. Recent advances in the improvement of g-C_3N_4 based photocatalytic materials. Chinese Chem. Lett. 32 (1), 13–20.
Xu, C.-Q., Zhang, W.-D., Deguchi, K., Ohki, S., Shimizu, T., Ma, R., Sasaki, T., 2020. Construction of a push-pull system in g-C_3N_4 for efficient photocatalytic hydrogen evolution under visible light. J. Mater. Chem. A 8 (26), 13299–13310.
Yan, L., Hou, J., Li, T., Wang, Y., Liu, C., Zhou, T., Jiang, W., Wang, D., Che, G., 2021. Tremella-like integrated carbon nitride with polyvinylimine-doped for enhancing photocatalytic degradation and hydrogen evolution performances. Sep. Purif. Technol. 279, 119766.
Yan, Z., Yin, K., Xu, M., Fang, N., Yu, W., Chu, Y., Shu, S., 2023. Photocatalysis for synergistic water remediation and H_2 production: a review. Chem. Eng. J. 472, 145066.
Yang, Y., Liu, J., Zhou, C., Zhang, P., Guo, S., Li, S., Meng, X., Lu, Y., Xu, H., Ma, H., Chen, L., 2019. In situ self-assembly synthesis of carbon self-doped graphite carbon nitride hexagonal tubes with enhanced photocatalytic hydrogen evolution. Int. J. Hydrogen Energ. 44 (50), 27354–27362.
Yang, Y., Li, X., Zhou, C., Xiong, W., Zeng, G., Huang, D., Zhang, C., Wang, W., Song, B., Tang, X., Li, X., Guo, H., 2020. Recent advances in application of graphitic carbon nitride-based catalysts for degrading organic contaminants in water through advanced oxidation processes beyond photocatalysis: a critical review. Water Res. 184, 116200.
Yang, X., Ma, J., Sun, S., Liu, Z., Sun, R., 2022. K/O co-doping and introduction of cyano groups in polymeric carbon nitride towards efficient simultaneous solar photocatalytic water splitting and biorefineries. Green Chem. 24 (5), 2104–2113.
Yang, H., Sun, S., Duan, R., Yang, B., Yang, M., Qi, X., Cai, C., Yun, D., Yang, Q., Cui, J., 2023. Mechanism insight into enhanced photocatalytic hydrogen production by nitrogen vacancy-induced creating built-in electric field in porous graphitic carbon nitride nanosheets. Appl. Surf. Sci. 631, 157544.

Yang, H., Sun, S., Lyu, J., Yang, Q., Cui, J., 2024. Mechanism insight into triple S-Scheme intermolecular carbon nitride homojunction with robust built-in electric field for highly enhanced photocatalytic hydrogen evolution. Chem. Eng. J. 481, 148297.
You, Q., Zhang, C., Cao, M., Wang, B., Huang, J., Wang, Y., Deng, S., Yu, G., 2023. Defects controlling, elements doping, and crystallinity improving triple-strategy modified carbon nitride for efficient photocatalytic diclofenac degradation and H_2O_2 production. Appl. Catal. B-Environ. 321, 121941.
Yu, D., Jia, T., Deng, Z., Wei, Q., Wang, K., Chen, L., Wang, P., Cui, J., 2022. One-dimensional P-doped graphitic carbon nitride tube: Facile synthesis, effect of doping concentration, and enhanced mechanism for photocatalytic hydrogen evolution. Nanomaterials 12 (10), 1759.
Yu, Y., Yan, W., Gao, W., Li, P., Wang, X., Wu, S., Song, W., Ding, K., 2017. Aromatic ring substituted g-C_3N_4 for enhanced photocatalytic hydrogen evolution. J. Mater. Chem. A 5 (33), 17199–17203.
Yuan, D., Chen, X., Li, Z., Fang, C., Ding, J., Wan, H., Guan, G., 2021. The impact of benzene ring embedding on the performance of carbon nitride for photocatalytic hydrogen. Appl. Surf. Sci. 569, 151089.
Zeng, X., Liu, Y., Kang, Y., Li, Q., Xia, Y., Zhu, Y., Hou, H., Uddin, M.H., Gengenbach, T. R., Xia, D., Sun, C., McCarthy, D.T., Deletic, A., Yu, J., Zhang, X., 2020a. Simultaneously tuning charge separation and oxygen reduction pathway on graphitic carbon nitride by polyethylenimine for boosted photocatalytic hydrogen peroxide production. ACS Catal. 10 (6), 3697–3706.
Zeng, X., Liu, Y., Xia, Y., Uddin, M.H., Xia, D., McCarthy, D.T., Deletic, A., Yu, J., Zhang, X., 2020b. Cooperatively modulating reactive oxygen species generation and bacteria-photocatalyst contact over graphitic carbon nitride by polyethylenimine for rapid water disinfection. Appl. Catal. B-Environ. 274, 119095.
Zeng, Y., Zhan, X., Hong, B., Xia, Y., Ding, Y., Cai, T., Yin, K., Wang, X., Yang, L., Luo, S., 2023. Surface atom rearrangement on carbon nitride for enhanced photocatalysis degradation of antibiotics under visible light. Chem. Eng. J. 452, 139434.
Zhang, J., Chen, Y., Wang, X., 2015. Two-dimensional covalent carbon nitride nanosheets: synthesis, functionalization, and applications. Energ. Environ. Sci. 8 (11), 3092–3108.
Zhang, Z., Chen, X., Zhang, H., Liu, W., Zhu, W., Zhu, Y., 2020b. A highly crystalline perylene imide polymer with the robust built-in electric field for efficient photocatalytic water oxidation. Adv. Mater. 32 (32), e1907746.
Zhang, H., Chen, X., Zhang, Z., Yu, K., Zhu, W., Zhu, Y., 2021. Highly-crystalline triazine-PDI polymer with an enhanced built-in electric field for full-spectrum photocatalytic phenol mineralization. Appl. Catal. B-Environ. 287, 119957.
Zhang, Q., Chen, J., Che, H., Wang, P., Liu, B., Ao, Y., 2022b. Recent advances in g-C_3N_4-based donor–acceptor photocatalysts for photocatalytic hydrogen evolution: an exquisite molecular structure engineering. ACS Mater. Lett. 4 (11), 2166–2186.
Zhang, Q., Chen, J., Gao, X., Che, H., Wang, P., Liu, B., Ao, Y., 2022c. Enhanced photocatalytic degradation of bisphenol A by a novel donor–acceptor g-C_3N_4: π-π interactions boosting the adsorption and electron transfer behaviors. Sep. Purif. Technol. 300, 121947.
Zhang, J.Y., Ding, J., Liu, L.M., Wu, R., Ding, L., Jiang, J.Q., Pang, J.W., Li, Y., Ren, N.Q., Yang, S.S., 2024. Selective removal of sulfamethoxazole by a novel double Z-scheme photocatalyst: Preferential recognition and degradation mechanism. Environ. Sci. Ecotechnol. 17, 100308.
Zhang, X., Ma, P., Wang, C., Gan, L., Chen, X., Zhang, P., Wang, Y., Li, H., Wang, L., Zhou, X., Zheng, K., 2022d. Unraveling the dual defect sites in graphite carbon nitride for ultra-high photocatalytic H_2O_2 evolution. Energ. Environ. Sci. 15 (2), 830–842.
Zhang, X., Li, M., Han, W., Wu, S.-E., Wang, H., Liu, S., Tang, Z., Zeng, L., 2023b. Recent advances in two-dimensional graphitic carbon nitride based photodetectors. Mater. Des. 235, 112405.
Zhang, C., Ouyang, Z., Yang, Y., Long, X., Qin, L., Wang, W., Zhou, Y., Qin, D., Qin, F., Lai, C., 2022a. Molecular engineering of donor-acceptor structured g-C_3N_4 for superior photocatalytic oxytetracycline degradation. Chem. Eng. J. 448, 137370.
Zhang, G., Savateev, A., Zhao, Y., Li, L., Antonietti, M., 2017. Advancing the n → π* electron transition of carbon nitride nanotubes for H2 photosynthesis. J. Mater. Chem. A 5 (25), 12723–12728.
Zhang, G., Wang, X., 2013. A facile synthesis of covalent carbon nitride photocatalysts by Co-polymerization of urea and phenylurea for hydrogen evolution. J. Catal. 307, 246–253.
Zhang, H., Xiao, Y., Peng, Y., Tian, L., Wang, Y., Tang, Y., Cao, Y., Wei, Z., Wu, Z., Zhu, Y., Guo, Q., 2023a. Selective degradation of ceftriaxone sodium by surface molecularly imprinted $BiOCl/Bi_3NbO_7$ heterojunction photocatalyst. Sep. Puri. Tech. 315, 123716.
Zhang, Y.X., Zeng, P., Yu, Y.X., Zhang, W.D., 2020a. Integration of nickel complex as a cocatalyst onto in-plane benzene ring-incorporated graphitic carbon nitride nanosheets for efficient photocatalytic hydrogen evolution. Chem. Eng. J. 381, 122635.
Zhao, T., Cheang, T.-Y., Chong, H.-B., Ling, C., Lu, X.-J., Li, C.-C., Fang, X.-X., Ma, L.-B., Wang, G., Xu, A.-W., 2021b. Biomolecular l-tryptophan as a hole mediator anchored on g-C_3N_4 exhibits remarkably enhanced photocatalytic H_2 evolution. Catal. Sci. Tech. 11 (14), 4776–4782.
Zhao, G., Li, B., Yang, X., Zhang, X., Li, Z., Jiang, D., Du, H., Zhu, C., Li, H., Xue, C., Yuan, Y., 2023. Two birds with one stone: Engineering polymeric carbon nitride with n-π* electronic transition for extending light absorption and reducing charge recombination. Adv. Powder Mater. 2 (1), 100077.
Zhao, S., Liu, Y., Wang, Y., Fang, J., Qi, Y., Zhou, Y., Liu, L., Zhuo, S., 2022. A self-assembly strategy to synthesize carbon doped carbon nitride microtubes with a large π-electron conjugated system for efficient H_2 evolution. Chem. Eng. J. 447, 137436.
Zhao, D., Wang, Y., Dong, C.-L., Huang, Y.-C., Chen, J., Xue, F., Shen, S., Guo, L., 2021a. Boron-doped nitrogen-deficient carbon nitride-based Z-scheme heterostructures for photocatalytic overall water splitting. Nature Energy 6 (4), 388–397.
Zhao, X., Zhang, Y., Zhao, X., Wang, X., Zhao, Y., Tan, H., Zhu, H., Ho, W., Sun, H., Li, Y., 2019. Urea and melamine formaldehyde resin-derived tubular g-C_3N_4 with highly efficient photocatalytic performance. ACS Appl. Mater. Inter. 11 (31), 27934–27943.
Zheng, Z., Tian, S., Feng, Y., Zhao, S., Li, X., Wang, S., He, Z., 2023. Recent advances of photocatalytic coupling technologies for wastewater treatment. Chinese J. Catal. 54, 88–136.
Zhong, S., Wang, Y., Li, S., Wang, S., Que, X., Sheng, L., Peng, J., Zhao, L., Yuan, L., Zhai, M., 2022. Enhanced photo-reduction of chromium(VI) from aqueous solution by nanosheet hybrids of covalent organic framework and graphene-phase carbon nitride. Sep. Purif. Technol. 294, 121204.
Zhou, T., Cui, F., Li, G., Sun, X., Sun, D., Liu, C., Zhao, C., Li, S., 2023a. Tailoring a sulfur doped carbon nitride skeleton to enhance the photocatalytic hydrogen evolution activity. New J. Chem. 47 (48), 22185–22191.
Zhou, Q., Guo, Y., Ye, Z., Fu, Y., Guo, Y., Zhu, Y., 2022a. Carbon nitride photocatalyst with internal electric field induced photogenerated carriers spatial enrichment for enhanced photocatalytic water splitting. Mater. Today 58, 100–109.
Zhou, T., Hou, J., Tai, M., Shi, J., Mi, X., Hu, B., Liu, C., Yan, L., Liu, L., 2023b. Polyethyleneimine-induced in-situ chemical epitaxial growth ultrathin 2D/2D graphene carbon nitride intralayer heterojunction with elevating photocatalytic activity: performances and mechanism insight. Int. J. Hydrogen Energ. 51, 884–896.
Zhou, C., Huang, D., Xu, P., Zeng, G., Huang, J., Shi, T., Lai, C., Zhang, C., Cheng, M., Lu, Y., Duan, A., Xiong, W., Zhou, M., 2019a. Efficient visible light driven degradation of sulfamethazine and tetracycline by salicylic acid modified polymeric carbon nitride via charge transfer. Chem. Eng. J. 370, 1077–1086.
Zhou, T., Li, T., Hou, J., Wang, Y., Hu, B., Sun, D., Wu, Y., Jiang, W., Che, G., Liu, C., 2022b. Tailoring boron doped intramolecular donor–acceptor integrated carbon nitride skeleton with propelling photocatalytic activity and mechanism insight. Chem. Eng. J. 445, 136643.
Zhou, C., Xu, P., Lai, C., Zhang, C., Zeng, G., Huang, D., Cheng, M., Hu, L., Xiong, W., Wen, X., Qin, L., Yuan, J., Wang, W., 2019b. Rational design of graphic carbon nitride copolymers by molecular doping for visible-light-driven degradation of aqueous sulfamethazine and hydrogen evolution. Chem. Eng. J. 359, 186–196.
Zhou, Z., Zhang, Y., Shen, Y., Liu, S., Zhang, Y., 2018. Molecular engineering of polymeric carbon nitride: advancing applications from photocatalysis to biosensing and more. Chem. Soc. Rev. 47 (7), 2298–2321.
Zhu, Y., Chen, Z., Gao, Y., Hu, C., 2020. General synthesis of carbon and oxygen dual-doped graphitic carbon nitride via copolymerization for non-photochemical oxidation of organic pollutant. J. Hazard Mater. 394, 122578.
Zong, X., Niu, L., Jiang, W., Yu, Y., An, L., Qu, D., Wang, X., Sun, Z., 2021. Constructing creatinine-derived moiety as donor block for carbon nitride photocatalyst with extended absorption and spatial charge separation. Appl. Catal. B-Environ. 291, 120099.